ROLE OF WARM ROLLING PROCESS ON THE CYCLIC STABILITY OF HIGH-HF CONTENT NITIHF SHAPE MEMORY ALLOYS

YÜKSEK HF İÇERİKLİ NİTİHF ŞEKİL HAFIZALI ALAŞIMLARIN ÇEVRİMSEL KARARLILIĞI ÜZERİNDEKİ SICAK HADDELEME İŞLEMİNİN ROLÜ

MUSTAFA YERLİTAŞ

PROF. DR BENAT KOÇKAR

Supervisor

Submitted to

Graduate School of Science and Engineering of Hacettepe University

as a Partial Fulfillment to the Requirements

for the Award of the Degree of Master of Sciences

in Mechanical Engineering.

2022

ABSTRACT

ROLE OF WARM ROLLING PROCESS ON THE CYCLIC STABILITY OF HIGH-HF CONTENT NITIHF SHAPE MEMORY ALLOYS

Mustafa YERLİTAŞ

Master of Sciences, Department of Mechanical Engineering
Supervisor: PROF. DR BENAT KOÇKAR
May 2022, 65 Pages

Shape Memory Alloys (SMAs) are special materials due to their shape recovery behaviors. SMAs remember their original shape after being deformed in their low temperature martensite phase and then heated back to their high temperature austenite phase. Thus, SMAs can be utilized as actuators in aerospace industry. NiTi based SMAs are widely used ones due to their high shape recovery and work output ability against applied load. However, their transformation temperatures (TTs) are lower than 100 ˚C and this limits their application area. There is a strong desire to increase TTs of SMAs for making them suitable candidates for high temperature applications. Nevertheless, as their working temperatures increase with the increase in TTs, the cyclic stability of the alloys starts to decrease due to the decrease in the resistance to plastic deformation via dislocation formation. As the martensite-austenite transformation takes place, dislocations, which are formed with the thermal and/or mechanical cycles pin the martensite/austenite boundary. Therefore, SMA is not able to demonstrate full shape recovery due to plastic deformation, which also leads to the presence of retained

martensite. There are several ways to raise TTs of NiTi binary alloys and to provide cyclic stability such as adding ternary element and applying heat treatments. The most promising additional element is Hf due to its lower cost and its effect in increasing the TTs to very high levels. Furthermore, it should be noted that NiTiHf ternary alloys are not only known as high temperature shape memory alloys (HTSMAs) but also high strength alloys.

In this study, $Ni_{50.1}Ti_{19.9}Hf_{30}$ (at%) was used due to its very high TTs and strength. Although NiTiHf alloys have very good properties as mentioned before, they lose these properties at high temperatures. Therefore, thermo-mechanical heat treatments were applied to very Hf-rich $Ni_{50.1}Ti_{19.9}Hf_{30}$ (at%) HTSMA to enhance its high temperature, functional and shape memory properties (SMPs). The alloy was first homogenized (H) and then warm rolled (WRed) at 3 different temperatures via following 2 different thickness reductions. Functional fatigue experiments (FFE) were conducted on homogenized and on each warm rolled sample. The effect of rolling temperature together with the percentage of thickness reduction on SMPs such as TTs (Austenite start (A_s) and finish (A_f), martensite start (M_s) and finish (M_f) temperatures), actuation (ε_{act}) and irrecoverable strains(ε_{irr}) was revealed by comparing the WRed samples with the H one. The hot extruded alloy was homogenized at 1050 ˚C for 2 hours and then the slices, which were cut from the extruded billet, were WRed at 500°C with 2% thickness reduction, at 800°C and 900°C with 10% thickness reduction.

TTs of all samples were measured by Differential Scanning Calorimetry (DSC) to determine the effect of warm rolling. Then FFEs were conducted using dog bone shape tensile specimens. The samples were loaded to 200MPa constant stress level and thermally cycled between 250°C and 700°C. All results, which were gathered from DSC and FFE, were compared.

One of the most promising findings in this study was the effect of warm rolling on the stability of the functional properties of $Ni_{50.1}Ti_{19.9}Hf_{30}$ (at%) alloy. Actuation strain (ε_{act}) values were found to be quite low but very stable throughout the FFE cycles. Moreover, TTs did not decrease significantly with warm rolling process.

Keywords: High Temperature Shape Memory Alloys, Functional Fatigue, Warm Rolling, Thermal Hysteresis, Transformation Temperatures, Actuation Strain

ÖZET

YÜKSEK HF İÇERİKLİ NITIHF ŞEKİL HAFIZALI ALAŞIMLARIN ÇEVRİMSEL KARARLILIĞI ÜZERİNDEKİ SICAK HADDELEME İŞLEMİNİN ROLÜ

Mustafa YERLİTAŞ

Yüksek Lisans, Makina Mühendisliği Bölümü
Tez Danışmanı: Prof. Dr. Benat KOÇKAR
Mayıs 2022, 65 Sayfa

Şekil Hafızalı Alaşımlar (ŞHA'lar), şekil geri kazanma davranışlarına sahip olmaları nedeniyle özel malzemelerdir. ŞHA'lar düşük sıcaklıktaki martensit fazında deforme olduktan sonra yüksek sıcaklıktaki östenit fazlarına geri ısıtıldıklarında başlangıç şekillerine geri dönebilir. Bu özelliklerinden dolayı, ŞHA'lar havacılık endüstrisinde eyleyici olarak kullanılabilirler. NiTi tabanlı ŞHA'lar, uygulanan yük karşısındaki yüksek şekil geri kazanım ve iş yapabilme özellikleri nedeniyle yaygın olarak kullanılır. Fakat dönüşüm sıcaklıklarının 100 ˚C'nin altında olması sebebiyle uygulama alanlarını kısıtlıdır. Bu alaşımların yüksek sıcaklık uygulamalarında kullanılabilmesi için dönüşüm sıcaklıklarının arttırılması büyük önem arz etmektedir. Bununla birlikte, dönüşüm sıcaklıkları arttıkça, plastik deformasyona karşı olan dirençlerinin azalması nedeniyle çevrimsel kararlılık azalmaya başlar. Martensit- östenit dönüşümü gerçekleştikçe termal ve/veya mekanik çevrimler sırasında oluşan dislokasyonlar martensit/östenit sınırının hareketini kısıtlar. Dönüşemeyen martensit oluşumuna sebep olan plastik deformasyon ŞHA'nın şeklini bütünüyle geri kazanmasını engeller. İkili NiTi şekil hafızalı alaşımların dönüşüm sıcaklıklarını yükseltmenin üçüncü element eklemek ve ısıl işlem uygulamak gibi birkaç yolu vardır. Düşük maliyeti ve dönüşüm sıcaklıklarının çok yüksek seviyelere çıkarmadaki etkisi nedeniyle gelecek vadeden element Hf'dir. Üçlü NiTiHf şekil hafızalı

alaşımların sadece yüksek sıcaklık şekil hafızalı alaşımlar (YSŞHA'lar) olarak değil, aynı zamanda yüksek mukavemetli alaşımlar olarak da bilinir.

Bu çalışmada, çok yüksek dönüşüm sıcaklıkları ve mukavemeti nedeniyle $Ni_{50.1}Ti_{19.9}Hf_{30}$ (at%) kullanılmıştır. Daha önce bahsedildiği gibi üçlü NiTiHf alaşımları çok iyi şekil hafıza özelliklere sahip olmalarına rağmen, yüksek sıcaklıkta bu özelliklerini kaybederler. Bu nedenle, yüksek sıcaklık, fonksiyonel ve şekil hafıza özelliklerini geliştirmek için Hf bakımından zengin $Ni_{50.1}Ti_{19.9}Hf_{30}$ YSŞHA'ya termo-mekanik ısıl işlemler uygulanmıştır. Alaşım önce homojenize edilmiş ve ardından 3 farklı sıcaklıkta 2 farklı kalınlık inceltme yüzdesi ile haddelenmiştir. Homojenize edilmiş ve termo-mekanik olarak işlem görmüş numunelerin her biri fonksiyonel yorulma deneylerine tâbi tutulmuştur. Haddeleme sıcaklığı ile kalınlık inceltme yüzdesinin; dönüşüm sıcaklıkları, eyleyici gerinimi ve geri dönüşemeyen gerinim gibi şekil hafıza özellikleri üzerine olan etkisi, homojenize edilmiş ve sıcak haddelenmiş numunelerin karşılaştırılması ile ortaya çıkartılmıştır. Sıcak ekstrüde edilmiş alaşım, 1050 ˚C'de 2 saat homojenize edildikten sonra homojenize edilmiş kütükten kesilen dilimler 500°C sıcaklıkta %2, 800°C ve 900°C sıcaklıklarda ise %10 kalınlıkta azalma sağlanarak sıcak haddelenmiştir.

Sıcak haddelenmenin etkisini belirlemek için, tüm numunelerin dönüşüm sıcaklıkları (Östenit Başlangıç, Östenit Bitiş, Martensit Başlangıç ve Martensit Bitiş sıcaklıkları) Diferansiyel Taramalı Kalorimetre (DTK) ile ölçülmüştür. Daha sonra köpek kemiği şeklindeki çekme numuneleri kullanılarak fonksiyonel yorulma deneyleri (FYD) gerçekleştirilmiştir. FYD'leri 200 MPa sabit gerilim altında ve 250°C ve 700°C arasındaki termal çevrimde yapılmıştır. DTK ve FYD'den elde edilen tüm veriler karşılaştırılmıştır.

Bu çalışmada gelecek vadeden bulgulardan birisi, sıcak haddelemenin $Ni_{50.1}Ti_{19.9}Hf_{30}$ (%at) alaşımının fonksiyonel özelliklerinin kararlı hale getirmesi üzerindeki etkisidir. Numunelerin eyleci gerinimlerinin FYD'deki çevrimler boyunca çok kararlı, eyleyici gerinim değerlerinin ise oldukça düşük olduğu saptanmıştır. Ayrıca, sıcak haddeleme işlemi sonrasında dönüşüm sıcaklıklarında önemli bir düşüş gözlemlenmemiştir.

Anahtar Kelimeler: Yüksek Sıcaklık Şekil Hafızalı Alaşımlar, Fonksiyonel Yorulma, Sıcak Haddeleme, Termal Histeresis Dönüşüm Sıcaklıkları, Eyleyici Gerinimi

ACKNOWLEDGEMENTS

First and foremost, I have to thank my supervisor Prof. Dr. Benat Koçkar. Without her assistance, guidance, and support in every step throughout the process, this study would have never been accomplished.

This study was supported by the Turkish Aerospace under Grant no. DKTM/2015/10, therefore, I would like to express my sincere gratitude.

I would like to thank to my all-lab mates in Hacettepe University Advanced Materials Laboratory for their support, assistance, and useful critiques, especially to Halil Onat Tuğrul, and Oğulcan Akgül.

I thank to my institution The Scientific and Technological Research Council of Turkey-Defense Industries Research and Development Institute for their support in providing academic leave for my master's degree.

I would like to express my special thanks to my father Celal Yerlitaş, my mother Dursun Yerlitaş, my brother Tolga Yerlitaş, my elder brother Osman Yerlitaş, his wife Ceylan Yerlitaş, my nephews Yusuf Sami and Ali Taylan for their support that they have always given to me.

Most importantly, none of this could have without my family. I thank to my wife Aylin and my lovely daughter Yasemin for always motivating and encouraging me to finish my master's degree in this very intense academic period.

TABLE OF CONTENTS

ABSTRACT ii

ÖZET v

ACKNOWLEDGEMENTS viii

TABLE OF CONTENTS ix

LIST OF FIGURES xi

LIST OF TABLES xiv

SYMBOLS AND ABBREVIATIONS xv

1. INTRODUCTION 1

2. THEORY AND LITERATURE 4

2.1. Shape Memory Alloy Types 6

2.1.1. Cu-based Shape Memory Alloys 6

2.1.2. Fe-based Shape Memory Alloys 6

2.1.3. NiTi-based Shape Memory Alloys 7

2.2. High Temperature Shape Memory Alloys (HTSMAs) 8

2.2.1. Ni-Ti-Hf HTSMAs 9

2.3. Effect of Thermo-mechanical Treatments on SMAs 13

2.3.1. Effects of Cold Rolling on NiTi based SMAs 16

2.3.2. Effect of Hot Rolling 18

3. EXPERIMENTAL PROCEDURE 21

3.1. As-Received Material 21

3.2. Homogenizing Heat Treatments 21

3.3. Warm Rolling 21

3.4. Sample Preparation 22

3.5. Differential Scanning Calorimetry (DSC) 23

3.6. Functional Fatigue Experiments 23

4. EXPERIMENTAL RESULTS AND DISCUSSION 25

4.1. Differential Scanning Calorimetry (DSC) Results 25
4.2. Functional Fatigue Experiments (FFE) 28
5. CONCLUSION 49
REFERENCES 51

LIST OF FIGURES

Figure 2.1-1. SMEs [17]. 4

Figure 2.1-2. Illustrated schematically Strain vs Temperature of an SMA, which shows the important SMPs[19]. 6

Figure 2.1-1. Results of compressed test in heating and cooling cycles for NiTiHf-based SMAs [24, 25, 28]. 8

Figure 2.2-1. Ni Content vs TTs in NiTiHf [43-46]. 11

Figure 2.2-2. Hf content vs TTs in NiTiHf alloys [43-46]. 12

Figure 2.2-3. Micro hardness evolution with Hf content in NiTiHf alloys [12]. 12

Figure 2.3-1. Transformation strain vs number of cycles for NiTiCu samples (annealing temp. 600℃ and annealing time 30 minutes) [48]. 14

Figure 2.3-2. Applied stresses vs number of cycles for NiTiCu samples (annealing temp. 600° C, annealing time 30 minutes and 500℃, 15 minutes) [48]. 15

Figure 2.3-3. SEM fractographies of two specimens, which were cycled under 250 MPa, fracture surface of the samples(a) which was aged for 1 hour at 450 °C(b) which was aged for 20 hours at 450°C [49]. 16

Figure 2.3-4. Hardness evolution of cold rolled NiTi samples as a function of thickness reduction [51]. 17

Figure 2.3-5. A comparison of the work output vs. FL responses of different alloys [53]. 18

Figure 2.3-6. a) The tensile true stress-true strain curves of the processed specimens (warm compressed samples) in comparison with the hot rolled one at room temperature, and b) the corresponding UTS and ductility [10]. 20

Figure 3.3-1. Thermo-mechanical process route summary in this study. 22

Figure 3.4-1. The dimensions of the dog bone tensile samples for FFEs. 23

Figure 3.6-1. The schematic of FF Test Setup [22]. 24

Figure 4.1-1. Tangent method to measure TTs from schematic heating and cooling curves [55] 26

Figure 4.1-2. Heating curves from DSC experiments for all samples. 26
Figure 4.1-3. Cooling curves from DSC experiments for all samples 27
Figure 4.2-1. Strain vs Temperature curves for H with the number of cycles. 29
Figure 4.2-2. Optical Images of Homogenized (H) Sample obtained by Optical Microscope at the end of (a) end of the70th cycle (b) end of the 110th cycle. 29
Figure 4.2-3. Optical Image of Homogenized (H) Sample obtained by Optical Microscope after 160th cycle (Last Cycle). 30
Figure 4.2-4. ε_{act} vs number of cycles for H, which were drawn using the data gathered during FFE. 31
Figure 4.2-5. Strain - Temperature responses for (H-WR2-500) obtained from FFE 33
Figure 4.2-6. Optical Images H-WR2-500 Sample, which were taken at the end of, (a) 50th Cycle (b) 110th Cycle (Last Cycle). 34
Figure 4.2-7. ε_{act} vs number of cycles for H-WR2-500 sample, which were drawn using the data gathered during FFE. 34
Figure 4.2-8. Evolution of TTs of H-WR2-500 sample with the number of cycles in FFE. 35
Figure 4.2-9. ε_{mar} and ε_{aus} (accumulated ε_{irr}) values as a function of cycles for H-WR2-500 sample, which were determined from strain -temperature curves of FFE. 36
Figure 4.2-10. Strain -Temperature responses of H-WR10-800. 37
Figure 4.2-11. ε_{act} vs number of cycles for H-WR10-800 sample, which were drawn using the data gathered during FFE. 38
Figure 4.2-12. Optical Images H-WR10-800 Sample, which were taken, **(a)** after warm rolling process and **(b)at** the end of 40th Cycle. 38
Figure 4.2-13. Optical Images H-WR10-800 Sample, which were taken at the end of, **(a)** 120th Cycle and **(b)** 150th Cycle (Last Cycle) 39
Figure 4.2-14. Evolution of TTs of H-WR10-800 sample with the number of cycles in FFE. 39
Figure 4.2-15. ε_{mar} and ε_{aus} (accumulated ε_{irr}) values as a function of cycles for H-WR10-800 sample, obtained from FFE. 41
Figure 4.2-16. Strain -Temperature response of H-WR10-900. 41

Figure 4.2-17. ε_{act} vs number of cycles for H-WR10-900 sample, which were drawn using the data gathered during FFE. 42
Figure 4.2-18. Optical Images H-WR10-900 Sample, which were taken **(a)** after 50^{th} cycle and **(b)** after 100^{th} cycle (Last Cycle). 43
Figure 4.2-19. Evolution of TTs of H-WR10-900 sample with the number of cycles in FFE. 43
Figure 4.2-20. ε_{mar} and ε_{aus} (accumulated ε_{irr}) values as a function of cycles for H-WR10-900 sample, which were determined from strain vs temperature curves of FFE. 45
Figure 4.2-21. Comparison of ε_{act} values of H, H-WR2-500, H-WR10-800, and H-WR10-900 samples. 46
Figure 4.2-22. Comparison of TTs of all samples, which are H, H-WR2-500, H-WR10-800, and H-WR10-900 (a) A_f and M_s (b) A_s and M_f. 47
Figure 4.2-23. Comparison of T_{hyst} values of all samples during FFE..... 47
Figure 4.2-24. Comparison of ε_{mar} and ε_{aus} (Total ε_{irr}) for all samples during the cycles of H, H-WR2-500, H-WR10-800, and H-WR10-900. 48

LIST OF TABLES

Table 4.1-1. TTs values obtained DSC. 27
Table 4.2-1. TTs with the cycle numbers of homogenized (H) sample. 32
Table 4.2-2. TTs with the cycle numbers of H-WR2-500 sample. 35
Table 4.2-3. TTs with the cycle numbers of H-WR10-800 sample 40
Table 4.2-4. TTs with the cycle numbers of H-WR10-900 sample 44

SYMBOLS AND ABBREVIATIONS

Symbols

ε_{act}	Actuation Strain
ε_{aus}	Austenite Strain
ε_{mar}	Martensite Strain
ε_{irr}	Irrecovarble Strain
Cu	Copper
Fe	Iron
Ni	Nickel
Ti	Titanium
Hf	Hafnium
T_{hyst}	Thermal Hysteresis

Abbreviations

A_s	Austenite Start Temperature
A_f	Austenite Finish Temperature
M_s	Martensite Start Temperature
M_f	Martensite Finish Temperature
DSC	Differential Scanning Calorimetry
SMA	Shape Memory Alloy
SMB	Shape Memory Behavior
SMP	Shape Memory Property
TT	Transformation Temperature
SME	Shape Memory Effect
FF	Functional Fatigue
FFE	Functional Fatigue Experiment
HTSMA	High Temperature Shape Memory Alloy
LCT	Lower Cycle Temperature
UCT	Upper Cycle Temperature
H	Homogenized

H-WR2-500	Homogenized and 2% Warm Rolled at 500 °C
H-WR10-800	Homogenized and 10% Warm Rolled at 800 °C
H- WR10-900	Homogenized and 10% Warm Rolled at 900 °C
WR	Warm Rolled
WRS	Warm Rolled Samples

1. INTRODUCTION

Shape Memory Alloys (SMAs) can exhibit a huge shape recovery against load due to phase transformation via heating-cooling cycle. They are deformed in their low temperature martensite phase and heated to high temperature austenite phase to observe the shape recovery. When SMAs are deformed in martensite phase twinned martensite transforms to detwinned martensite and the most convenient martensite variant grows at the expense of the other variants. Therefore, the shape change appears. When the alloys are heated at which above A_f, detwinned martensite transforms to austenite and the alloys recover the shape change and transform back to their original shape. Therefore, they are very promising materials for actuator applications in aerospace industry [1-6].

There are several critical parameters in SMAs applications such as ε_{act}, TTs, fatigue life (FL) and thermal hysteresis (T_{hyst}). Stability of these parameters is significant during actuation cycles. Therefore, stability of the aforementioned parameters should be considerably sustained during life cycles.

Nickel Titanium binary alloys are the most preferred SMAs among Cu and/or Fe based SMAs due to their high strength and outstanding shape memory abilities. However, TTs of Ni-Ti alloys are lower than 100 ˚C [5-7]. Therefore, Ni-Ti based SMAs cannot be used for high temperature applications [8]. Adding third or more elements to Ni-Ti alloys is one of the methods to increase TTs. As the TTs increase, thus the operating temperatures increase, thermal and mechanical stabilities become questionable since plastic deformation takes place at high operating temperatures [1].

In actuation applications in aerospace industry, it is required to have TTs above 100 °C with maintaining the actuation stabilities [9]. There have been many studies focused on this topic. The alloys, which have TTs higher than 100°C are named as High Temperatures SMAs (HTSMAs).

Adding ternary element to NiTi based SMAs is a common method to increase the TTs as mentioned above [1]. In the literature, Hf, Zr, Pd, Pt and Au were used as ternary

elements. Au, Pd an Pt are more expensive than Zr and Hf, so they are not cost friendly. Zr makes the alloy brittle [10-13]. Therefore, Hf is more promising as a ternary element for high temperature applications.

The TTs of NiTi based SMAs are strongly dependent on composition of the alloys [14]. For example, the TTs of Ni lean binary NiTi alloy (Ni content < 50%) are relatively higher [15] than that of NiTi alloys having a bit more 50 at% of Ni and as Hf concentration increases in NiTiHf ternary alloys, TTs increase almost linearly as well [7]. Additionally, Hf concentration should be higher than 10% to observe the increase in TTs in ternary NiTiHf alloys.

There were many studies on deformation of NiTi based SMAs in the literature. It was known that deformations such as rolling (warm or cold), and extrusion increase dislocation density and reduce grain size. It is also known that when dislocation density increases or grain size decreases, the critical shear stress for slip increases not only in structural metal alloys but also in SMAs [13] . Therefore, to maintain the cyclic stability during thermo-mechanical cycles at high temperatures, increasing the strength of alloys is the main motivation of the researchers working on HTSMAs.

This study focuses on that role of warm rolling process on the cyclic stability of $Ni_{50.1}Ti_{19.9}Hf_{30}$ that has very high Hf content. It is worth to mention that the composition of the alloy is given in at%. Besides, the effects of rolling temperature and reduction in sample thickness on SM properties of the alloy have been investigated. Up to author's best knowledge this is first study on the warm rolling studies of $Ni_{50.1}Ti_{19.9}Hf_{30}$.

All of the samples used in this study were homogenized before warm rolling processes and then WRed at 500°C with 2% thickness reduction and at 800 and 900°C with 10% thickness reduction. The samples, which were homogenized and WRed, thermally cycles under 200 MPa to investigate the effect of warm rolling process to fatigue life and to the evolution of the actuation properties of the alloy throughout cycles. It was observed that low temperature rolling with low thickness reduction did not significantly affect the actuation behavior of HTSMA that was used in this study, but noticeable stability in

actuation properties was achieved via warm rolling at 800°C and 900°C with 10% thickness reduction.

2. THEORY AND LITERATURE

Shape Memory Effect (SME) is a phenomenon that occurs when a deformed material is heated and then returns to it is original shape. SMAs are capable of doing work via returning to their original shapes under applied load. NiTi SMA was discovered at 1960s by United States Naval Ordnance Laboratory (NOL) and it was industrialized with the name of Nitinol (Ni-Ti). However, shape memory related phenomena superelasticity was previously discovered in AuCd alloy in 1932 [16].

When SMA is loaded at low temperature (at martensite phase), twinned martensite transforms to detwinned martensite and thus the shape change is attained. Then, the load is released, detwinned martensite structure remains. Detwinned martensite is heated to a temperature higher than A_f and transformation is occurred from martensite to austenite and the alloy remembers its first shape at the beginning. This transformation routine is demonstrated in Figure 2.1-1.

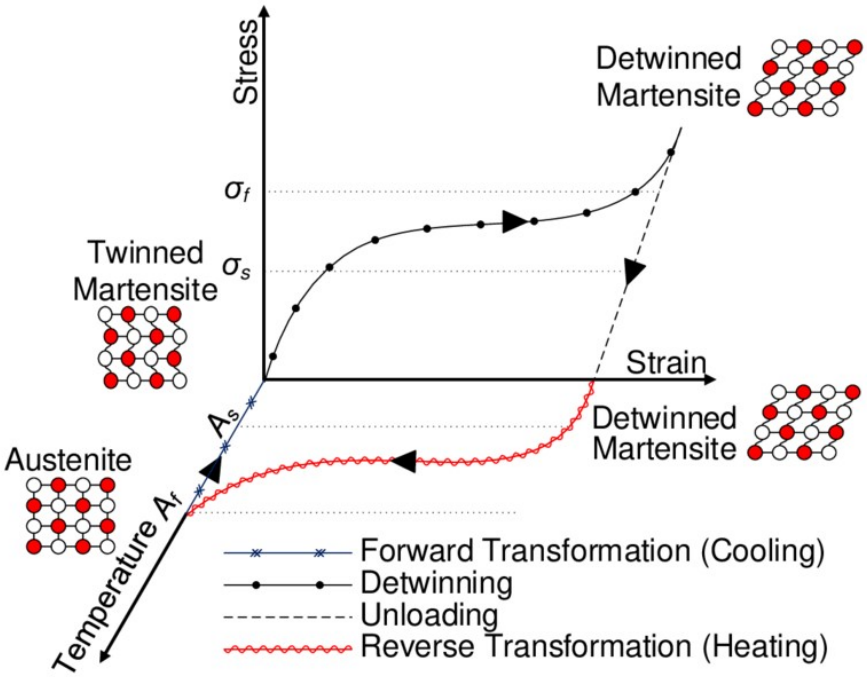

Figure 2.1-1. SMEs [17].

Compared to other alloy systems, NiTi shape memory alloys (SMAs) show decent dimensional stability, SM properties and ductility at room temperature [1, 4-6, 15, 18]. Ni-Ti application areas of SMAs are spread out as automotive, aerospace, and medical industries by means of the fact that they have high strength and large reversible shape changes [1-4, 6, 15].

There are some crucial parameters to determine the appropriate application areas of SMAs. These parameters are TTs, ε_{act}, ε_{act}, and T_{hyst}, which are schematically shown in Figure 2.1-1. This figure is a common strain vs temperature graph for SMAs, which is obtained from cooling-heating experiments under applied constant load. These kinds of experiments are named as isobaric or load-biased cooling-heating experiments in the literature. There are four TTs (A_s, A_f, M_s and M_f) shown in Figure 2.1-2. The temperatures at which beginning and ending of transformation of Austenite phase are shown as A_s and A_f, respectively. Also, the temperatures at which beginning and ending of transformation of Martensite are shown as M_s and M_f, respectively. The T_{hyst} is defined as the measure of the difference between the mid-points of martensite and austenite transformation curves as shown on the graph [6]. Martensite strain (ε_{mar}) corresponds to the strain magnitude when the SMA fully transforms to Martensite as shown in Figure 2.1-2. ε_{irr} and corresponds to the difference in strain values between the heating curve and cooling curve at approximately A_f+50°C due to the incomplete shape recovery. Accumulation of ε_{irr} values happening at the end of each cooling and heating cycle is defined as Austenite Strain (ε_{aus}) in the literature.

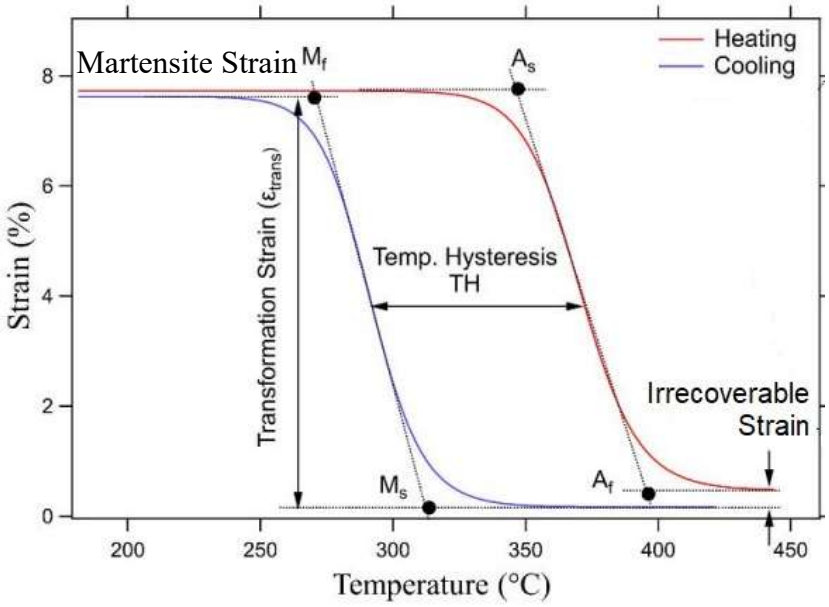

Figure 2.1-2. Illustrated schematically Strain vs Temperature of an SMA, which shows the important SMPs[19].

2.1.Shape Memory Alloy Types

Although there are different types of categorization approaches SMAs are categorized in 3 groups based on their elemental content. They are Cu-based, Fe-based and NiTi-based SMAs.

2.1.1. Cu-based Shape Memory Alloys

One of the important properties of this group alloy is their relatively lower TTs compared to the other types of SMAs. TTs of Cu-Zn SMAs are below -50 ˚C where TTs of Cu-Al SMAs are above 100 °C [20], [21]. Most well-known Cu-based SMAs are these Cu-Zn and Cu-Al type SMAs. TTs are one of the most significant properties for SMAs, which dictate their utilization in applications. Cu-Zn-Al, Cu-Al-Mn and Cu-Al-Ni are greatest subject to study in Cu-based ternary SMA systems. Cu-based ternary SMAs have better superelastic behavior than that of the other ternary SMA types, but they have low cyclic stability due to their tendency to plastic deformation [14, 22].

2.1.2. Fe-based Shape Memory Alloys

First of all, it is worth to mention that Fe-based SMAs are cost efficient. Also, the SMPs of Fe-based SMAs are lower than that of Cu-based and NiTi-based SMAs. Fe-Ni-Co-Ti,

Fe-Pt and Fe-Pd alloys have low T_{hyst} that are less than 10°C. Other Fe-based SMAs such as Fe-Mn-Si and Fe-Ni-C show T_{hyst} of around 150˚C [23]. Since the T_{hyst} of these alloys are high, they are not preferred for actuation applications. Adding Ni, Co or Cr elements to Fe-Mn-Si alloys is promising due to the strength increase with the addition of forth element. However, these alloys also have high T_{hyst} values. As a result, they are not suitable SMAs for actuation applications in aerospace industry but are preferred to be utilized in the area of damping, vibration control actively and prestressing/posttensioning of civil engineering applications.

2.1.3. NiTi-based Shape Memory Alloys

NiTi SMAs are the most popular alloys thanks to their dimensional stabilities, ductility, and their corrosion resistance. However, TTs of NiTi are similar to other binary SMAs and below 100 °C. Therefore, they are not appropriate for high temperature applications at which TTs are desired 100°C and above [8].

Figure 2.1-1 shows the effect of Nb and Pd additions on SM properties of NiTiHf SMAs. Several studies show that quaternary SMAs are high strength materials compared to ternary SMAs. However, they are generally brittle, causing the application areas to be limited. Adding Pd to NiTiHf, the strength and the stability of SMA increase but the alloy shows less actuation strain and TTs are decreased with Pd addition. On the contrary, adding Nb to NiTiHf increases ductility of the alloy but decreases TTs [24-27].

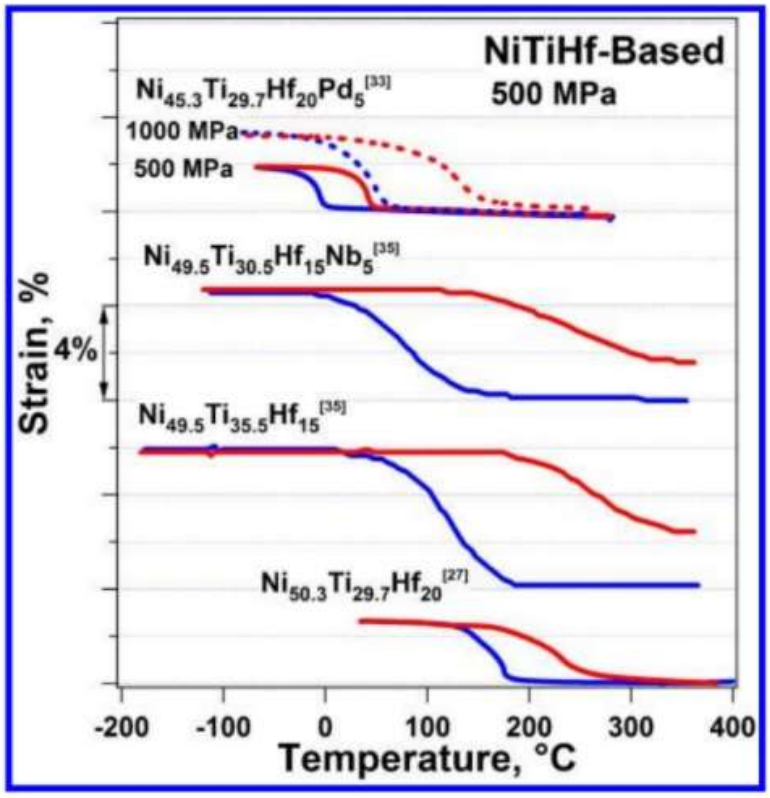

Figure 2.1-1. Results of compressed test in heating and cooling cycles for NiTiHf-based SMAs [24, 25, 28].

2.2.High Temperature Shape Memory Alloys (HTSMAs)

SMAs based on Ni-Ti are widely used in automotive, aerospace, and medical industries due to the fact that Ni-Ti SMAs have high strength and large reversible shape change [1,4]. However, they are not preferred which is used at high temperature environments as aforementioned. Since their TTs are lower than 100 ˚C, they are not suitable for the high temperature actuator applications (higher than 100˚C)[8]. To increase the TTs of NiTi binary alloys, adding ternary elements such as Hf, Zr, Pd, Pt, and Au is necessary. Au, Pd an Pt elements are more expensive than that of Hf. In addition to this, to use Zr as the ternary element makes SMAs brittle. Thus, Hf added NiTi alloys are the ternary alloys, which are the most suitable ones for the actuator applications at high temperatures [10-13].

Some problems are stated for HTSMAs in many studies. The most important drawback of HTSMAs is their cyclic instability. They are utilized at high operating temperatures, therefore their critical shear strength for slip (CRSS) values decrease. Since CRSS

decreases, plastic deformation with dislocation formation takes place during Martensite-Austenite phase transformation via heating-cooling under stress or loading-unloading at constant temperature.

To tackle with the plasticity problem, thermal, mechanical, or thermo-mechanical treatments can be utilized to improve the stability of SM properties via increasing their dislocation formation resistance. There are significant methods such as work and precipitation hardening to enhance the strength of SMAs. Work hardening with applying deformation processes such as rolling, extrusion and drawing lead to an increase in plastic deformation resistance of these alloys due to the increase in deformation induced dislocations. If the dislocation density is increased tremendously then the alloys become brittle, and this may lead to observe early failure. To overcome this problem, subsequent annealing treatments can be done, or deformation processes can be applied at relatively higher temperatures. However, it should be stated that the annealing and/or deformation process temperature value is a critical parameter to control the dislocation formation or grain size evolution. The process temperature should be low enough to obtain enough dislocations to rise the alloy's strength yet high enough to rearrange dislocation formations to obtain enough ductility and shape recovery [1, 29]. For, example, if the annealing after deformation process is applied at very high temperatures the recovery and recrystallisation take place and strengthening cannot be achieved or if the annealing is applied at very low temperature, then the partial recovery of the ductility cannot be attained.

2.2.1. Ni-Ti-Hf HTSMAs

SMAs are used as actuators and/or morphing components in aircraft and space vehicles due to many advantages such as being light weight [2, 30-33].

There are several developments about SMAs, such as their applications in medical and petroleum industries, but SMAs usage in aerospace industry has grown slower than that of other industrial implementations due to their low cyclic stability [9, 34-36].
SMAs are used as actuators in aerospace applications since SMAs can easily be adapted to different flight stages by adjusting the TTs. Additionally, the shape recovery against applied load can be sustained for many cycles after increasing their resistance to plastic

deformation, so, the actuation system can be robust and reliable. The designs of aerodynamic components such as wings become more flexible and light weight due to utilizing SMAs as actuators instead of using heavy weight engine type of actuators. However, architectures of the designs need to be optimized for working under higher aerodynamic loads [37].

Ni-Ti based SMAs are the most preferred alloys in actuator applications due to having high strength and superior SMPs, however TTs are lower than 100 °C. Therefore, they are not suitable to be used in high operating temperature environment [38]. As mentioned before, "Hf, Zr, Pd, Pt, and Au elements" are added to increase TTs and adding Hf is the most promising one thanks to cost efficiently and achieving great TTs together with relatively higher ductility [6-8, 14, 22].

The reason of NiTiHf as primary HTSMAs in aerospace applications is having promising SMPs such as stable T_{hyst} and higher TTs [13, 39, 40]. NiTiHf HTSMAs should retain their mechanical stability at high temperature applications; however, it is also known that strength of all metal alloys decreases at high temperatures. As the strength decreases in HTSMAs, plastic deformation occurs and thus, the cyclic stability becomes a problem. ε_{act} decreases and the ε_{irr} during cycles. To overcome the stability problem, there is a necessity to apply thermal or thermo-mechanical treatments to these alloys such as aging or rolling, extrusion and/or any other deformation processes. Precipitation hardening via aging heat treatment and strain hardening via applying deformation processes lead to increase in resistance of the alloy against plastic deformation and hence the cyclic stability can be achieved [41].

NiTiHf alloys can be classified depending on Ni-content which are Ni-rich and Ni-lean. Ni-lean means that Ni content in SMAs is lower than 50 at% and Ni-rich means Ni content is more than 50 at% of the alloy. TTs remain constant up to 50 at% of Ni but when Ni content increases above 50 at% in NiTiHf alloys (Ni-rich), TTs suddenly decrease. There are many studies about effects of Ni content and Hf content in NiTiHf alloys. Figure 2.2-1 represents that relationship between Ni content in $Ni_xTi_{90-x}Hf_{10}$ alloys and TTs [42].

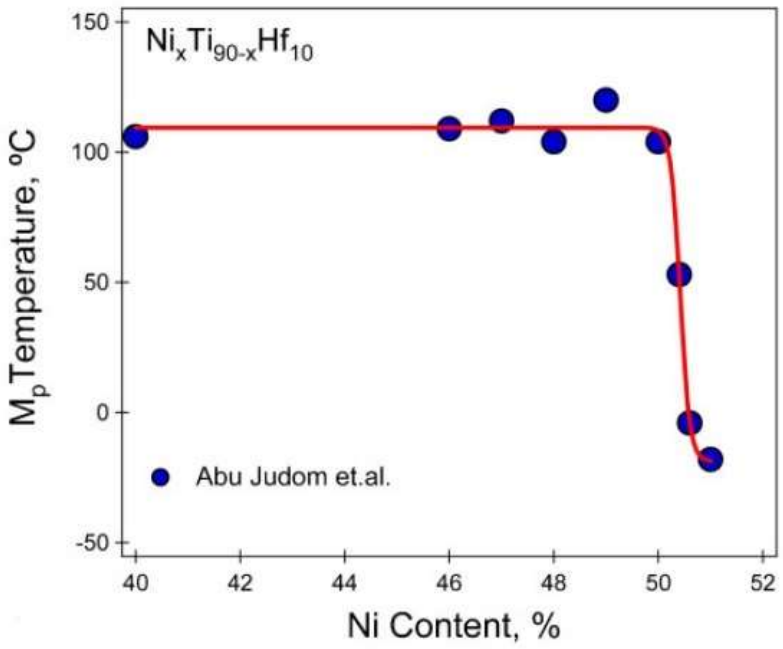

Figure 2.2-1. Ni Content vs TTs in NiTiHf [43-46].

TTs are affected by Hf content in NiTiHf alloys as well. It is obvious that Hf content is a function of TTs as shown in Figure 2.2-2. There were many research groups working on the TT evolution regarding Hf content as it is illustrated in Figure. These studies show that TTs are not significantly changing by increasing Hf content until 5%. Martensite peak temperature increases tremendously after adding 5 at% of Hf [43-46].

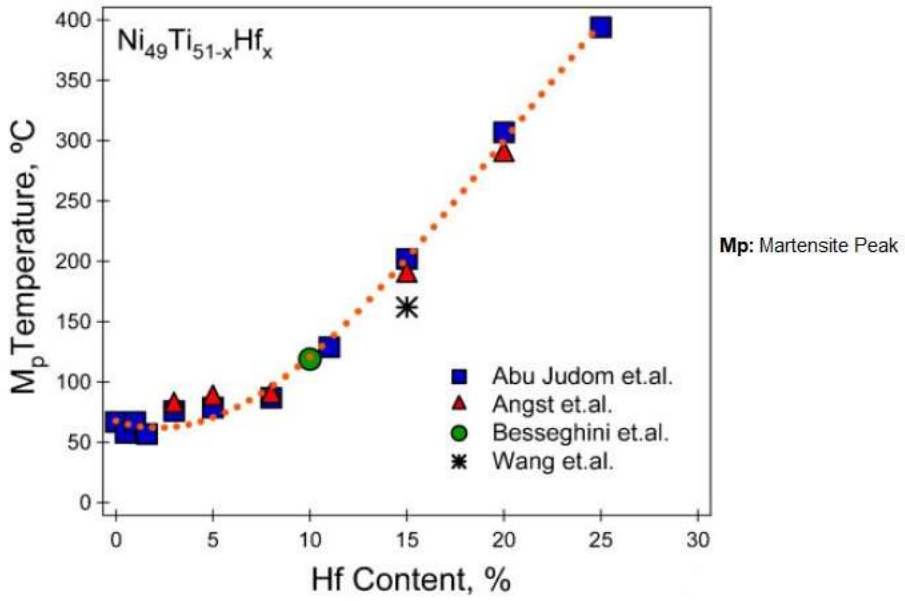

Figure 2.2-2. Hf content vs TTs in NiTiHf alloys [43-46].

Additionally, increasing Hf content in the NiTi alloys also leads to an increase in the hardness as shown in Figure 2.2-3.

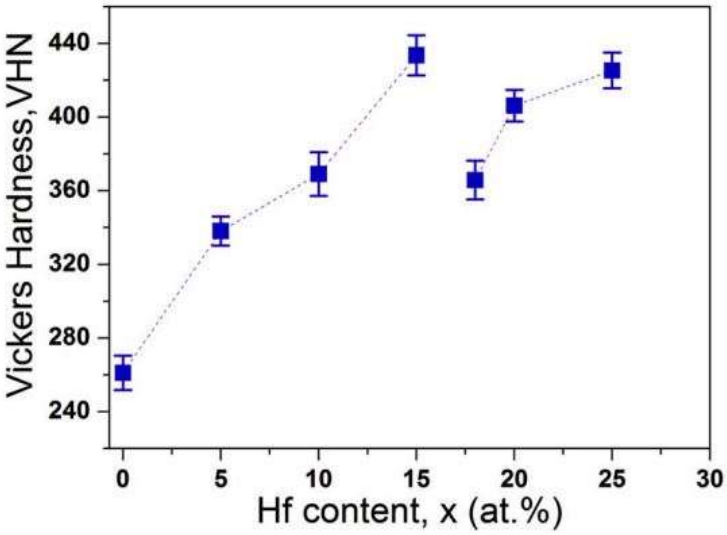

Figure 2.2-3. Micro hardness evolution with Hf content in NiTiHf alloys [12].

2.3.Effect of Thermo-mechanical Treatments on SMAs

In various applications such as medicine and aerospace industry, SMAs are used in forms of tubes, rods, wires, and thin structures [47]. Therefore, plastic deformation methods are used for giving different forms to SMAs. Several thermal, mechanical, and thermo-mechanical treatments can be applied on SMAs such as rolling, drawing, aging, annealing and homogenizing. All these processes lead to a change in the SMPs of SMAs. For instance, when NiTiHf alloys which have Ni content higher 50% are aged higher TTs, strength and cyclic stability of all SMPs can be attained. The reason of the increase in TTs is because of the precipitate formation and these precipitates lead to a decrease in the Ni-content of the matrix which leads to an increase in TTs as shown in Figure 2.2-1.

Cold-warm-hot rolling and/or mechanical or thermo-mechanical deformation processes induce internal stresses and increase the dislocation density not only in SMAs but also in all metal alloys. Martensite and austenite TTs are decreased with increasing deformation percentage because of inducing higher internal stress and dislocation density. The dislocations pin the martensite-austenite boundary, so, the transformation is hindered due to this pinning effect. To overcome this effect, the alloys should be overcooled to observe the martensitic transformation. Therefore, especially Martensitic TTs decrease.

There are two types of fatigue approach those are worth to investigate in SMAs which are structural and functional. Structural fatigue is defined as the decrease in material's strength with the crack initiation and propagation during periodic loading cycles. Finally, the fracture occurs due to the decreased load bearing capacity of the material with the decrease in the cross-sectional area. On the other hand, FF is the deterioration of the SMPs such as actuation behavior with the increase in dislocation density and decrease in transforming volume. Actuation behavior can be lost, and failure occurs with the number of loading-unloading at constant temperature (superelastic cycling) or heating-cooling cycles under applied stress (shape memory cycles).

Lagoudas and his co-workers investigated how heat treatment temperature and time together with the applied stress magnitude affect fatigue life (FL) of NiTiCu. Figure 2.3-2 represents that FL decreased with increasing applied stress and transformation strain was inversely proportional with FL [48]. This study was conducted on two samples. One of

which was annealed at 550 °C for 15 min. and the other one was annealed at 600 °C for 30 min. Figure 2.3-2 demonstrated that annealed specimen at 550 °C in 15 minutes had higher FL under at the same stress level than that of the other one [48].

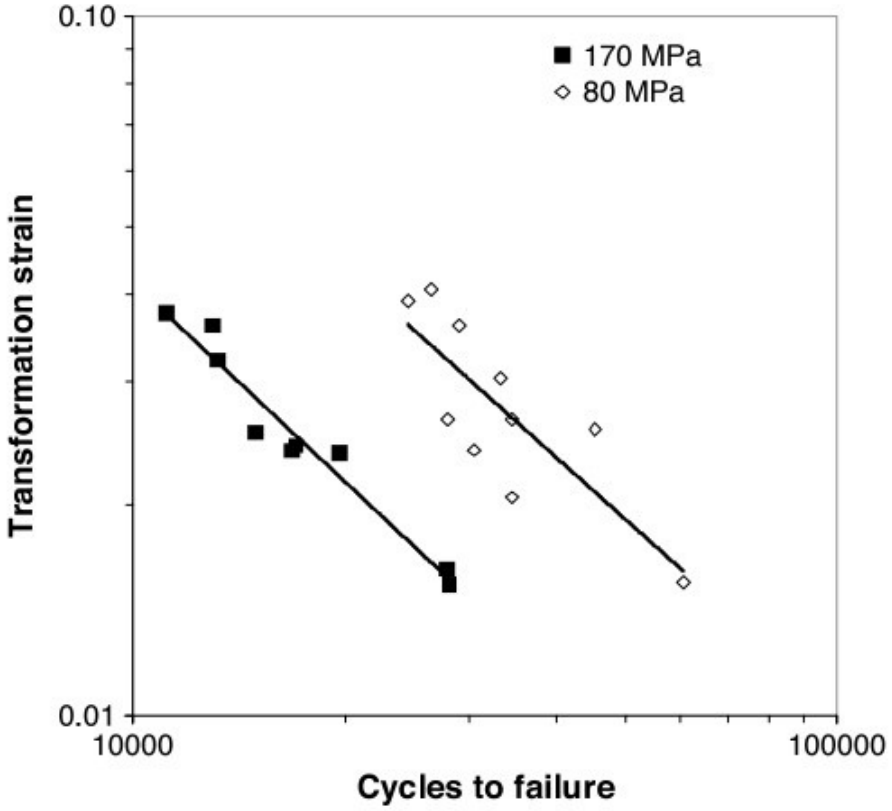

Figure 2.3-1. Transformation strain vs number of cycles for NiTiCu samples (annealing temp. 600℃ and annealing time 30 minutes) [48].

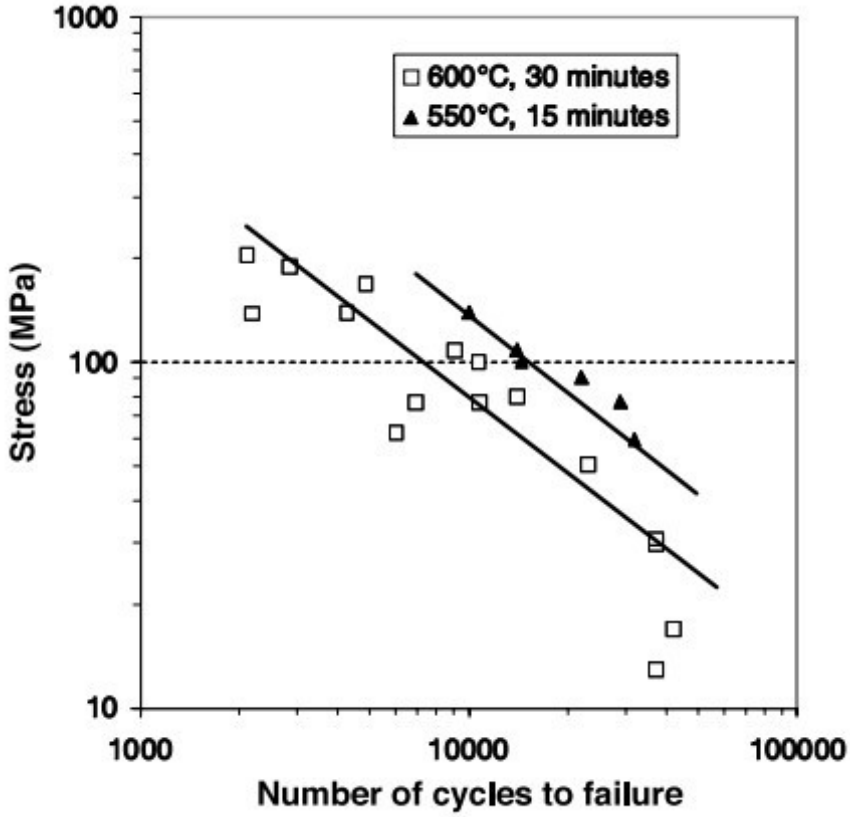

Figure 2.3-2. Applied stresses vs number of cycles for NiTiCu samples (annealing temp. 600° C, annealing time 30 minutes and 500°C, 15 minutes) [48].

Olivier W. Bertacchinia et. al. studied the relationship between aging time and fatigue response of $Ni_{60}Ti_{40}$. Two different aging time (1 hour and 20 hours) and one aging temperature (450 °C) were selected in this study. The results of this study appeared that two specimens' FL were nearby 4000 cycles under 250 MPa. The fracture surfaces of the samples, which were aged at 450°C for 1hr and 20hrs, after running the cycles under 250MPa, were illustrated in Figure 2.3-3 (a) and (b). The one, which was aged for 1 hour became brittle in the final stage of the cyclic experiment and the other one, which was aged for 20 hours became ductile in the final stage[49].

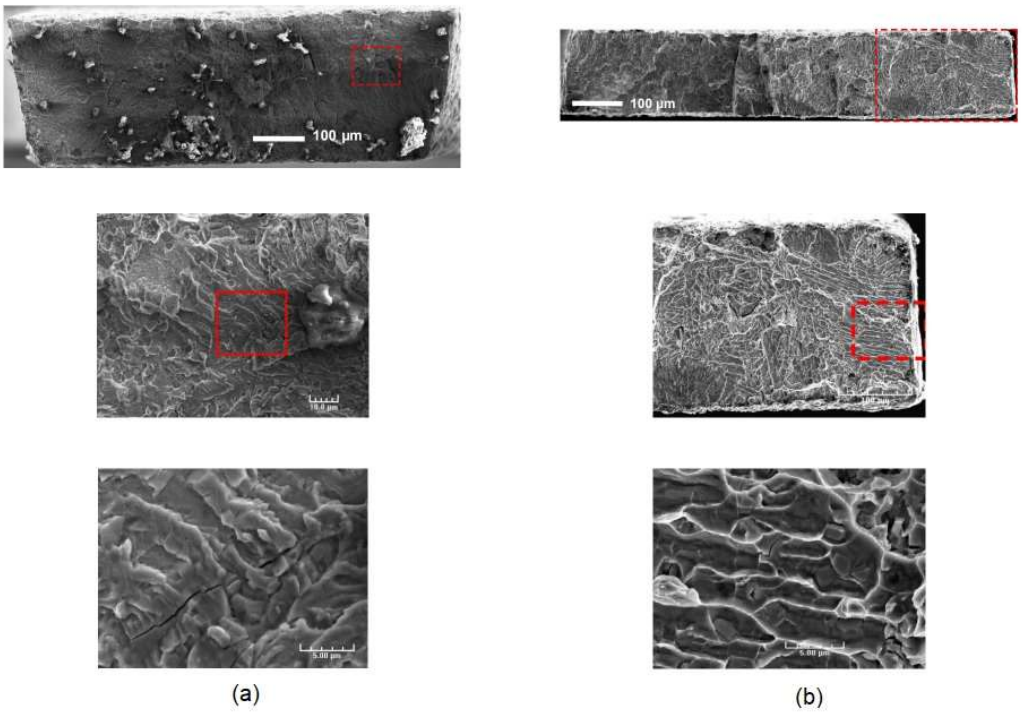

Figure 2.3-3. SEM fractographies of two specimens, which were cycled under 250 MPa, fracture surface of the samples(a) which was aged for 1 hour at 450 °C(b) which was aged for 20 hours at 450°C [49].

Ni-rich NiTiHf HTSMAs are precipitation hardenable alloys such that plasticity can be reduced with the formation of nanoprecipitates [9]. Yet, equiatomic NiTiHf alloys are not precipitation hardenable therefore, they can be strengthened only by following deformation processes through strain hardening via rolling, extrusion, or forging.

2.3.1. Effects of Cold Rolling on NiTi based SMAs

There have been many studies about cold rolling on SMAs which were conducted by different research teams.

Kockar's group showed that cold rolling and aging process of $Ni_{50.3}Ti_{29.7}Hf_{20}$ had a high impact on TTs, ε_{act}, ε_{irr}, and T_{hyst} values. The results of the experiments demonstrated that cold rolling process led to observe stable TTs and ε_{act} values, even though ε_{act} values obtained from cold rolled sample were found to be less than that of hot extruded sample. As a result, thermomechanical treatments are useful methods to improve the stability of SMPs of the alloys [13] .

Slip deformation instead of twinning during Austenite to Martensite transformation under applied load may take place, therefore SMAs show permanent shape change instead of full shape recovery. Plastic deformation, in other terms, dislocation accumulation takes place with the number of cooling-heating cycles under applied load. V.G. Pushin et.al. investigated that plastic deformation methods (cold roll i.e.) are used to achieve fine grain structures and higher dislocation density in Ni-Ti based SMAs. Plastic deformation methods significantly improve the strength since grain size were decreased and dislocation density was increased after plastic deformation, hence, the cyclic endurance of shape memory and pseudo-elasticity behavior of these alloys was enhanced via decreasing plastic deformation during austenite to martensite transformation [26].

Hosoda et al. discovered that increasing reduction in thickness by cold rolling leads to obtain harder NiTi alloys. The reason of the increase in hardness is the increase in the number of dislocations that were formed during cold rolling process [50].Increase in hardness values is highly related with the thickness reduction in cold rolling process as shown in Figure 2.3-4 [51].

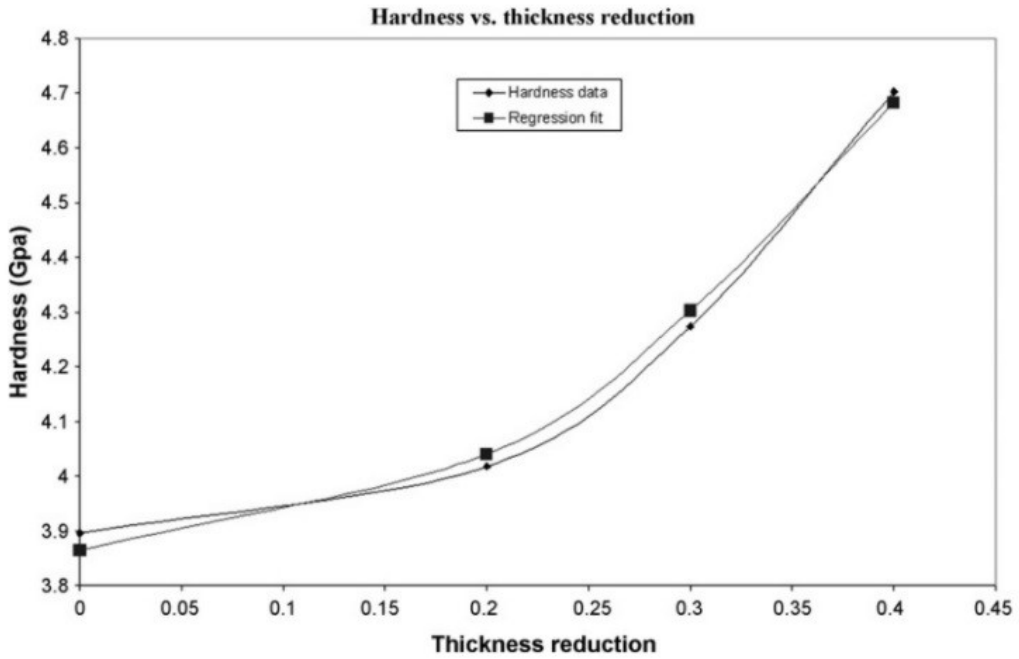

Figure 2.3-4. Hardness evolution of cold rolled NiTi samples as a function of thickness reduction [51].

Ley's group worked on NiTi based SMAs as well and investigated that cold rolling is a promising method to achieve the desired high strength, hardness, and the suitable recoverable strains in these alloys [52].

Karakoc et. al. investigated the actuation fatigue response of nanoprecipitation hardened $Ni_{50.3}Ti_{29.7}Hf_{20}$ HTSMA in thermal cycling from martensite to austenite under different constant tension load magnitudes. Figure 2.3-5 shows the relationship between aging time and temperatures, FL, and applied stress values for different NiTi-based alloys. The applied stress values affect the actuation response of the HTSMAs, especially the ε_{act}, ε_{irr}, and FL. When the stress was raised, FL was decreased but at the same time ε_{act} was increased [53].

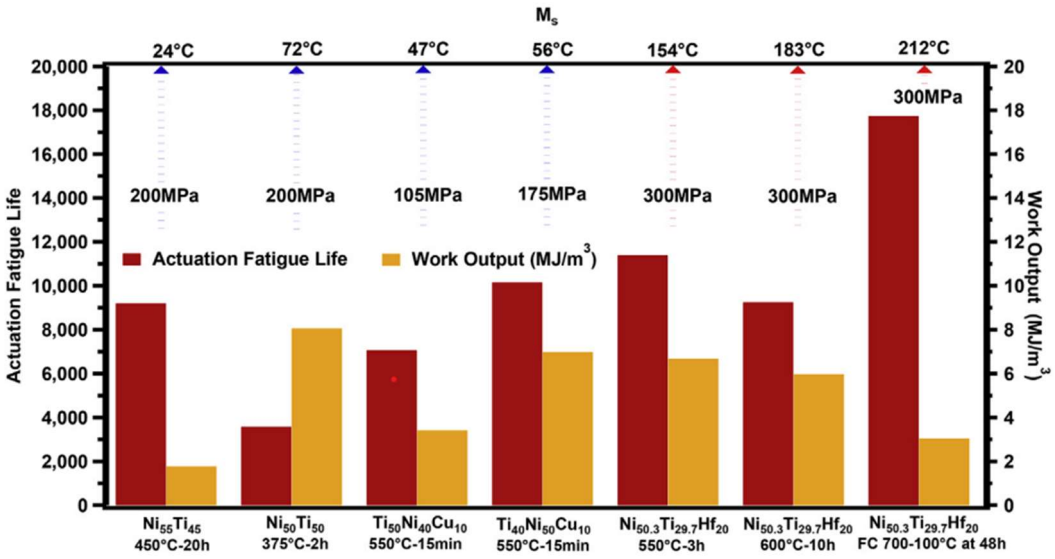

Figure 2.3-5. A comparison of the work output vs. FL responses of different alloys [53].

2.3.2. Effect of Hot Rolling

There have been many studies which were conducted by different research groups. As mentioned in previous sections, thermo-mechanical treatments are applied on HTSMAs to enhance SMPs. Hot rolling is one another thermo-mechanical treatment which is generally preferred when the alloy is a hard to deform material. NiTiHf SMAs are hardly deformable materials such that it is a challenge to roll them at relatively low temperatures. Alloy becomes relatively ductile at higher temperatures, therefore, rolling deformation with higher thickness reduction and without crack formation becomes possible.

There is a basic difference between hot and cold rolling treatments. Cold rolling leads to achieve higher dislocation density and rolling texture and thus affects the transformation properties of SMAs, whereas hot rolling has less effect on transformation characteristics since high temperature inhibits the formation of very amount of dislocation and texture. A. Ahadi and his co-workers investigated how microstructure of a near-equiatomic NiTi SMAs is affected after hot rolling process. The study showed that the grain size was decreased, and dislocation density was increased when the thickness reduction was raised from 30% to 50%. There was an observation about mechanical twinning formation during hot rolling at 800 °C and this was determined to be the dominant deformation mechanism, on the other hand, when the alloy was hot rolled at 700 °C mechanical twinning did not exist. Therefore, the rolling temperature is a significant parameter in the rolling procedure.[54]

Babacan et.al. showed "the effects of cold and warm rolling on near-equiatomic $Ni_{50}Ti_{30}Hf_{20}$ HTSMAs" [11]. It was concluded that the optimum SMPs were achieved with the application of cold rolling and the subsequent annealing process. 550 ˚C for 30 mins was stated as the optimum aging parameters [11]. When annealing temperature changed, TTs were altered accordingly. If annealing temperature was kept between 450 ˚C and 550 ˚C, TTs decreased.

As the annealing temperature was raised to 600 ˚C, M_f and A_s temperatures increased with respect to the TTs, which were obtained after cold rolling, as well. They showed that cold rolling and subsequent annealing and warm rolling improved the martensitic transformation reversibility and the dimensional stability of the near-equiatomic $NiTiHf_{20}$ HTSMAs, so these SMAs can be used for high-temperature actuator applications. In addition, cold rolling and subsequent annealing led to observe better cyclic stability than that of the one observed with the application of warm rolling in this HTSMA [11]. However, it is worth to mention that this study did not consider the long-term fatigue cycles. They ran only 100 cycles to evaluate the effect of cold and warm rolling processes.

Ataei, et.al. studied effects of warm compression process on the mechanical properties of Ni-Ti based alloys. When warm compression was conducted on SMAs, the strength as well as the ductility were enhanced at the same time. Therefore, this thermomechanical

treatment could be considered as a capable alternative method to cold working and subsequent annealing to enhance the cyclic shape recovery of the alloys.

Figure 2.3-6 presents the mechanical test results of the warm compressed samples at different temperatures and with different strain rates. In this study, samples were warm compressed at 300 °C and 500 °C under strain rates of 0.3 and 0.003 s^{-1}. These samples were named as 300-0.3, 300-0.003, 500-0.3 and 500-0.003. The first numbers (300, and 500) represent compression temperature and the other numbers (0.3, and 0.003) represent strain rate in Figure 2.3-6 [10].

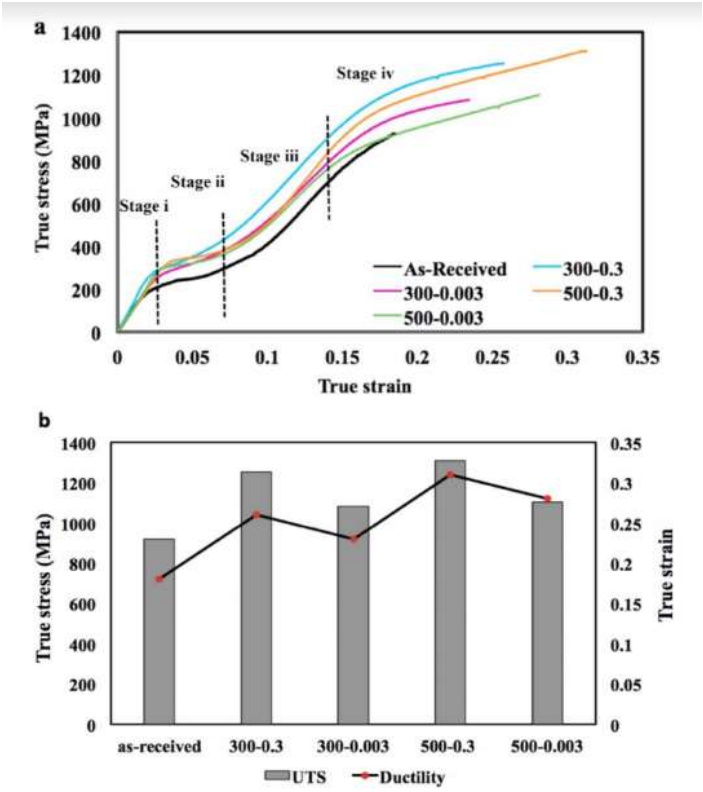

Figure 2.3-6. a) The tensile true stress-true strain curves of the processed specimens (warm compressed samples) in comparison with the hot rolled one at room temperature, and b) the corresponding UTS and ductility [10].

3. EXPERIMENTAL PROCEDURE

3.1.As-Received Material

$Ni_{50,1}Ti_{19,9}Hf_{30}$ (at%) HTSMA was produced in using high-purity Ni, Ti, and Hf elements via vacuum induction melting (VIM). The cast billet was then hot extruded at 900 ˚C, with an area reduction of 4:1 after it was sealed in mild steel to decrease the friction between the extrusion die and the material and to prevent the oxidation during the hot extrusion process. Steel layer around the extruded rod was removed by the turning process after hot extrusion.

3.2.Homogenizing Heat Treatments

A piece from the extruded alloy was cut and covered by tantalum foil to prevent potential oxidation during the homogenizing process. A cylindrical furnace –was purged using high purity argon gas and used for this heat treatment. Homogenization temperature was 1050 ˚C and the duration for homogenization was selected as 2 hours. $Ni_{50,1}Ti_{19,9}Hf_{30}$ alloy has high oxygen affinity. Therefore, relatively high temperature and short time were chosen to minimize risk of potential oxidation. Argon was also used as protective gas in the process to prevent further oxidation of the alloy.

3.3.Warm Rolling

The homogenized piece of alloy was sliced with Wire Electron Discharge machining (WEDM) technique for warm rolling operations. The thickness of each slice was approximately 1.05mm. WEDM residue layers of the slices were removed by smooth grinding. Warm rolling was conducted at 500˚C with 2% thickness reduction, at 800˚C and 900˚C with 10% thickness reduction. Samples were heated in a cubic furnace before the rolling process. Thus, warm rolling was performed non-isothermally. Homogenized sample is indicated by the letter H, and warm rolled samples are indicated by the letters WR in the text of the thesis. In total, 4 thermo-mechanically treated samples were investigated in this study with the indications H, H-WR2-500, H-WR10-800, and H-WR10-900. The numbers after the letters WR indicate the thickness reduction and the

numbers at the end of the codes indicate the rolling temperature. Homogenizing process was applied on all samples.

Figure 3.3-1 illustrares the summary of the operation routes, which was followed on all samples.

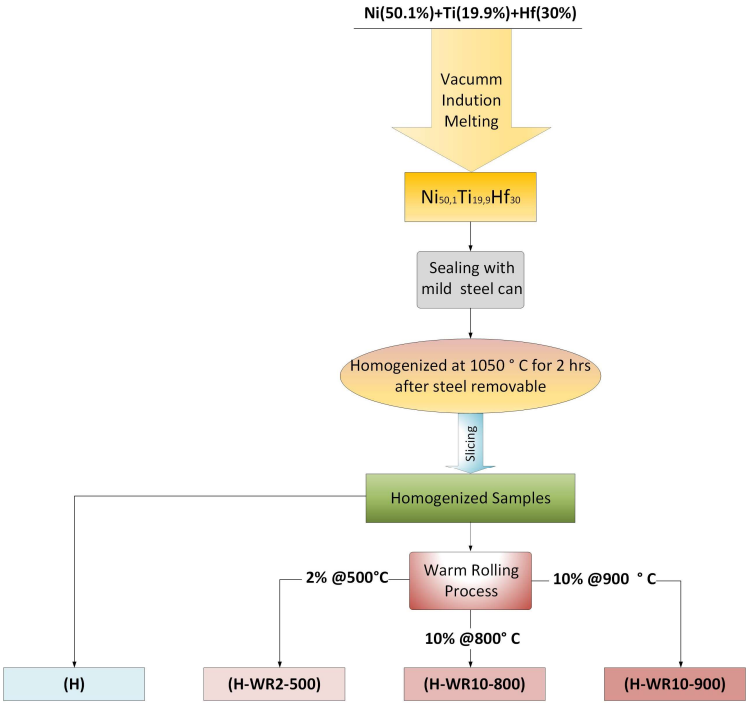

Figure 3.3-1. Thermo-mechanical process route summary in this study.

3.4.Sample Preparation

FF specimens were cut by using WEDM as dog bone tensile samples. The gage length, width and thickness of the dog bone samples were 16.6 mm, 2.25 mm, and 1 mm, respectively. The schematic of the samples is shown in Figure 3.4-1. The samples for Differential Scanning Calorimetry experiments to measure TTs of each sample were cut by saw precision cutter at very low speed rates and without applying load to rule out inducing stress via mechanical cutting. Cutting induced stress may lead to observe unexpected TT values at the first heating cycles in DSC experiments. Water was also used as coolant during cutting operations.

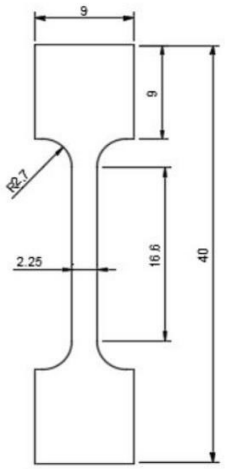

Figure 3.4-1. The dimensions of the dog bone tensile samples for FFEs.

3.5.Differential Scanning Calorimetry (DSC)

TTs measurements of all thermo-mechanical treated $Ni_{50,1}Ti_{19,9}Hf_{30}$ (at%) samples were made by "DSC- Perkin Elmer 8000" under no load conditions. The thermal cycles were conducted between 300°C and 700°C with constant heating and cooling rates of 10°C/min. Two cycles were run to observe a possible change in TTs with the cycles. Nitrogen gas was used as the protective gas in DSC tests.

3.6.Functional Fatigue Experiments

FFEs were carried out with specifically designed and custom-built FF test setup. Firstly, to the load value corresponding to 200 MPa constant stress was calculated by considering the cross-sectional area of the samples. Since the temperature measurement was done by "Optris CT laser LTF-CF1" infrared thermometer, the emissivity value should be known. Therefore, FF samples were sprayed a heat resistant black paint to accurately measure the temperature of the sample since the emissivity value of black color is known. Heating process was carried out with the electric current passing through samples via DC power supply. The samples were cooled by natural convection. The displacement measurements were made with a linear potentiometric displacement sensor (LPDS). FFEs were run under 200 MPa constant stress. Samples were heated to the austenite phase, and then load was hung. Thermal cycles were started via cooling the sample to 250°C and heating to 700°C. The heating and cooling rates were set constant as 15 °C/sec in all experiments.

The lower and upper temperature limits, which are called as Lower Cycle Temperature (LCT) and Upper Cycle Temperature (UCT), respectively, of the thermal cycles were set as 250°C and 700°C due to TTs of the samples, which were measured by DSC. Heating-cooling rates and the temperature limits were controlled via PI controller. The National Instruments LabView Program was used to gather the data during cycles and temperature and displacements data were collected for each cycle.

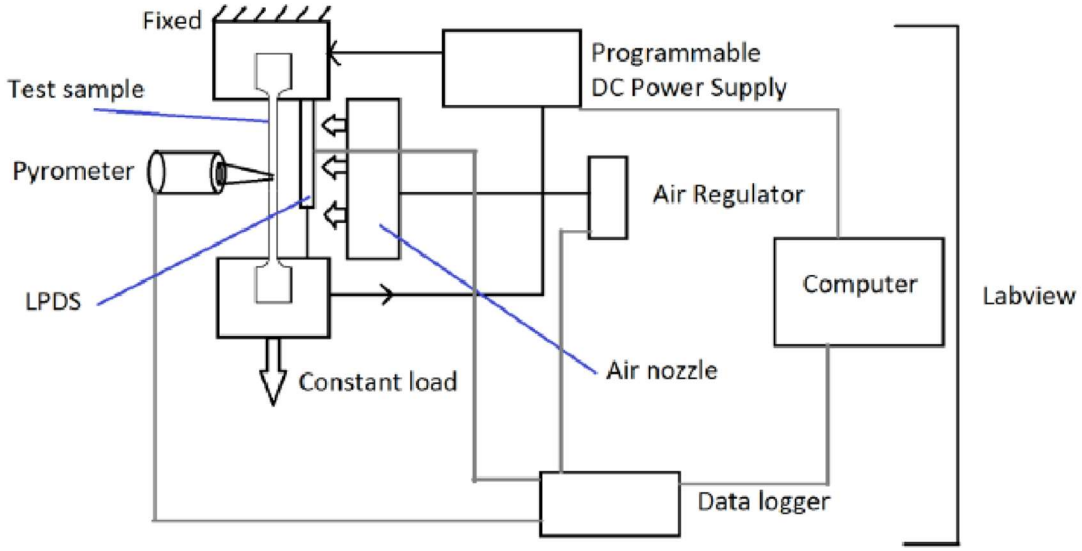

Figure 3.6-1. The schematic of FF Test Setup [22].

4. EXPERIMENTAL RESULTS AND DISCUSSION

4.1.Differential Scanning Calorimetry (DSC) Results

The tangent method, which was applied to find out A_f, A_s, M_s and M_f, is shown in Figure 4.1-1. The heating and the cooling cycles of DSC curves of H, H-WR2-500, H-WR2-800, and H-WR10-900 samples are illustrated in Figure 4.1-2 and Figure 4.1-3, respectively. In addition, Table 4.1-1 shows TTs of all samples, which were drawn from 1st and 2nd heating-cooling cycles of DSC curves. First of all, it is worth to mention that all TTs comparisons are done with respect to H, hence, the H can be referred to as the base sample. A_f decreased after warm rolling operations as shown in Table 4.1-1. On the other hand, warm rolling did not lead to a significant change in A_s temperature. Additionally, M_s temperature showed decreasing tendency with warm rolling and the decrease was significant when the thickness reduction was increased from 2% to 10%. It was impossible to determine M_f temperature of H-WR10-800 sample since the cooling curve for this sample is very broad. However, M_f temperature decreased after warm rolling the sample at 500°C with 2% thickness reduction and then increased by raising the rolling temperature to 900°C although the thickness reduction was raised to 10% as well. Generally speaking, A_f and M_s decreased with the warm rolling operation and the warm rolling effect was found to be more pronounced on the evolution of M_s temperature. There are 2 possible reasons for this pronounced decrease in M_s temperature. One is the dislocation density increase with the rolling operation and the second is the possible oxidation during heating the sample. The large decrease in M_s temperature with the increase in rolling temperature can be based on oxidation as well as the increase in the thickness reduction.

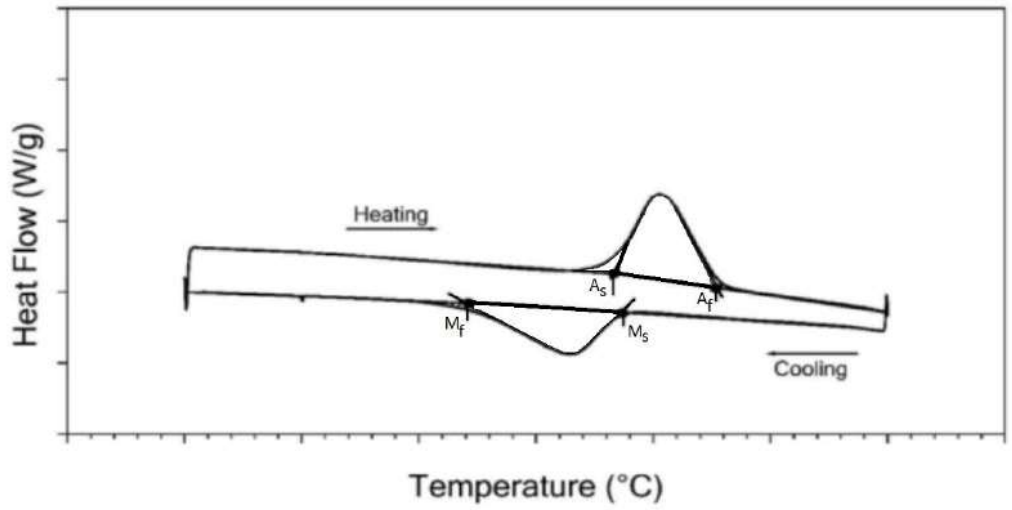

Figure 4.1-1. Tangent method to measure TTs from schematic heating and cooling curves [55].

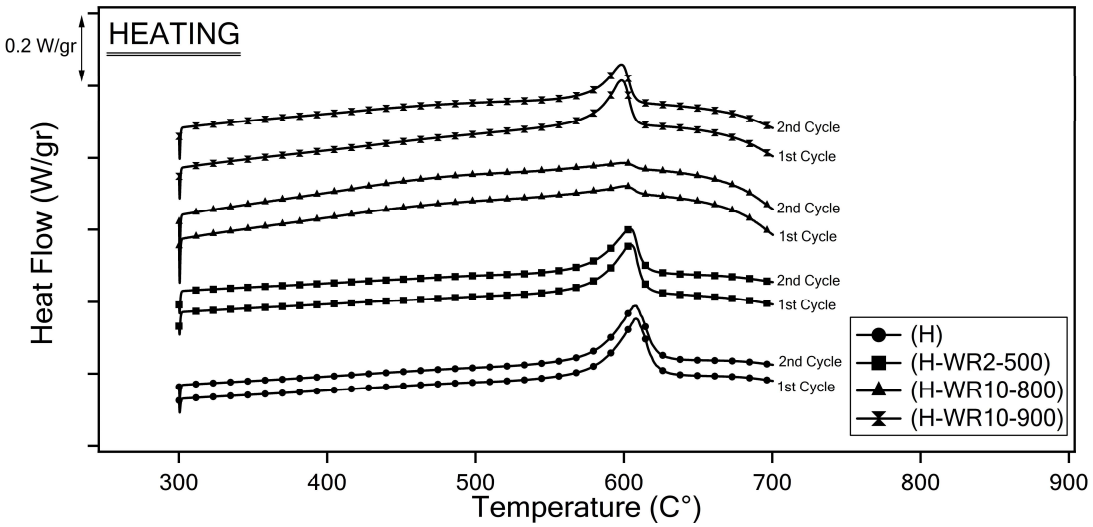

Figure 4.1-2. Heating curves from DSC experiments for all samples.

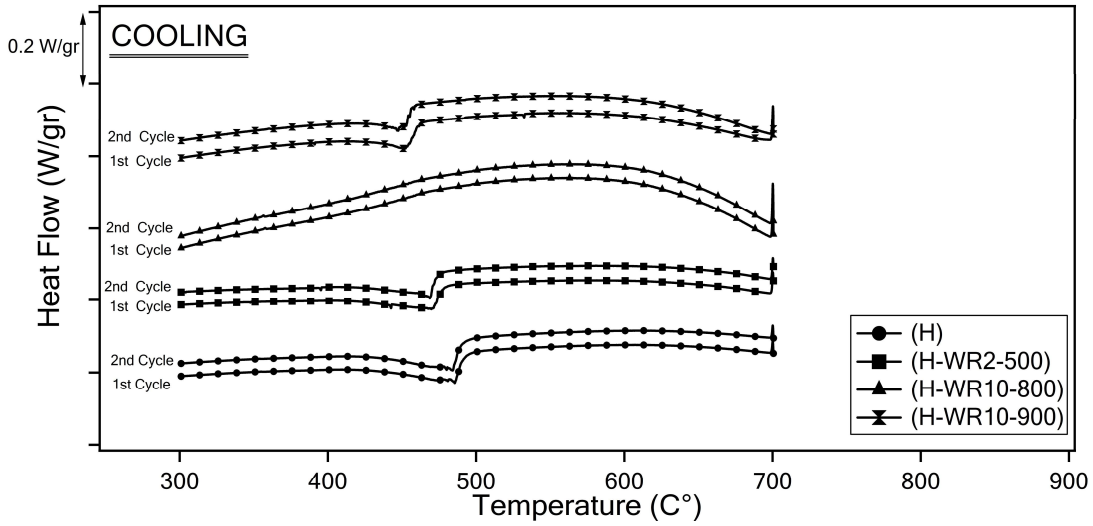

Figure 4.1-3. Cooling curves from DSC experiments for all samples.

Table 4.1-1. TTs values obtained DSC.

Sample Name	Cycle	M_f (°C)	M_s(°C)	A_s (°C)	A_f (°C)
H	1	430.89	493.25	575.09	623.35
	2	432.95	492.42	576.28	623.36
	Difference(°C) (Cycle 2-1)	2.06	-0.83	1.19	0.01
H-WR2-500	1	418.73	481.16	573.29	617.58
	2	418.67	474.5	576.41	614.78
	Difference (°C) (Cycle 2-1)	-0.06	-6.66	3.12	-2.8
H-WR10-800	1	-	463.24	584.58	610.64
	2	-	470.87	577.87	611.35
	Difference (°C) (Cycle 2-1)	-	7.63	-6.71	0.71
H-WR10-900	1	437.39	461.88	572.27	607.61
	2	433.69	457.03	575.04	608.24
	Difference (°C) (Cycle 2-1)	-3.7	-4.85	2.77	0.63

4.2.Functional Fatigue Experiments (FFE)

FFEs were performed under constant 200 MPa. Upper cycle temperature (UCT) is a very significant input parameter for FFE since the strength of metal alloys decreases at high temperature and therefore UCT should be kept as low as possible but should be enough for full recovery of the shape change. UCT was determined based on the data obtained from DSC experiments and the samples were heated approximately 50 to 80°C above A_f temperature. It was known from previous studies in the literature that increasing operating temperatures decreases the FL of HTSMAs due to the decrease in strength. On the other hand, ε_{act} increases by setting higher UCT since relatively higher martensite to -austenite transformation occur at local regions. Revealing the effect of UCT on SMPs was not the aim of this study, thus, UCTs were set to a constant value for all samples. The main scope of the study is the role of the warm rolling process on the cyclic stability of high-Hf content $Ni_{50.1}Ti_{19.9}Hf_{30}$ (at%) HTSMA. Therefore, FFEs were conducted on H, H-WR2-500, H-WR10-800, and H-WR10-900 samples.

As mentioned in the previous section that, strain and temperature data were collected throughout all FFEs and strain vs. temperature curves were drawn for all samples to determine the SMPs such as ε_{act}, ε_{mar}, and ε_{aus} as well as the TTs. The procedure to determine, ε_{mar}, ε_{aus}, and ε_{act} and the TTs were given at the first part of the Theory Section and in Figure 2.1-2.

First of all, FFE was conducted on H and all the FFE results were compared by taking the H properties into consideration and to clear the effect of warm rolling process on FF response of $Ni_{50.1}Ti_{19.9}Hf_{30}$ (at%) HTSMA. The strain-temperature curves of H sample with the number of cycles are shown in Figure 4.2-1.

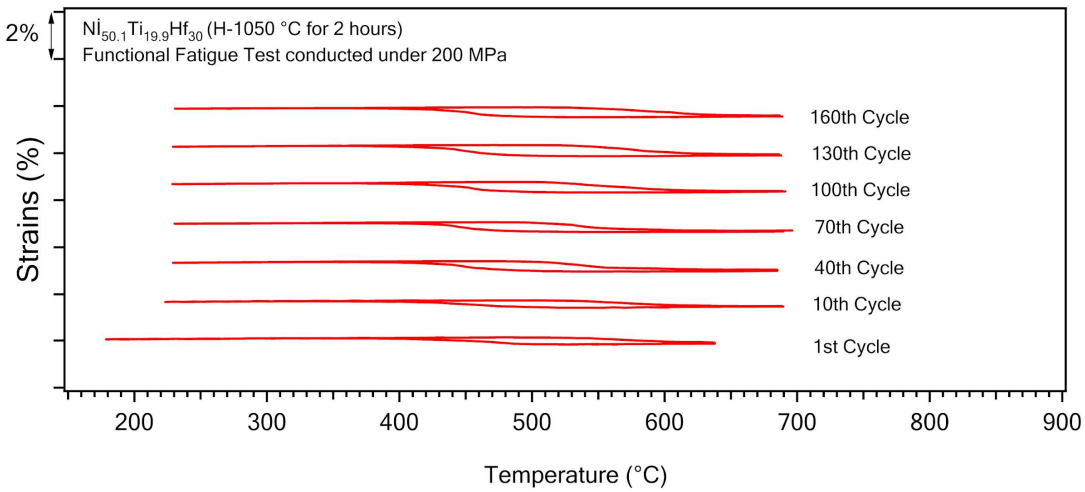

Figure 4.2-1. Strain vs Temperature curves for H with the number of cycles.

The crack formations and propagation behavior of the cracks were represented with optical microscope images, which were taken after 70, 110 and 160 cycles, are shown in Figure 4.2-2 and Figure 4.2-3. It is clear to see that as the cycle number increased the length and the width of the cracks increased.

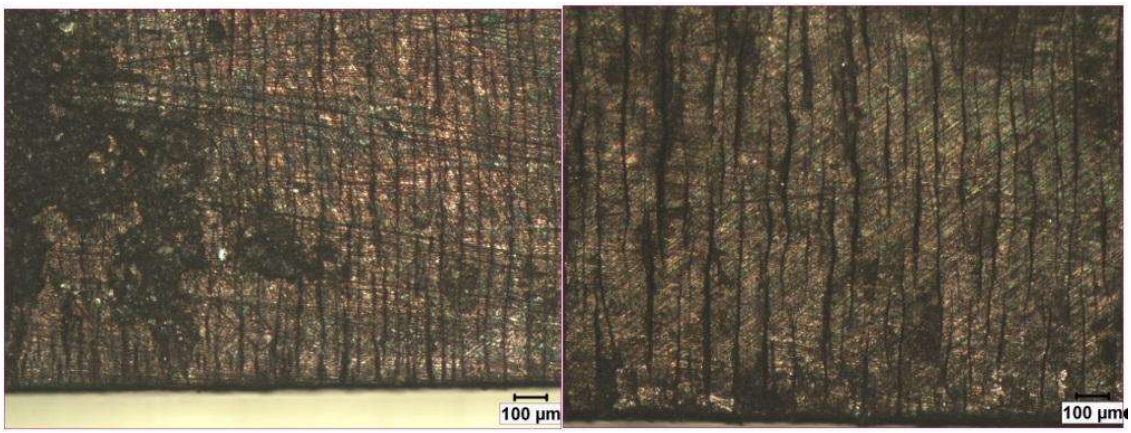

Figure 4.2-2. Optical Images of Homogenized (H) Sample obtained by Optical Microscope at the end of (a) end of the70th cycle (b) end of the 110th cycle.

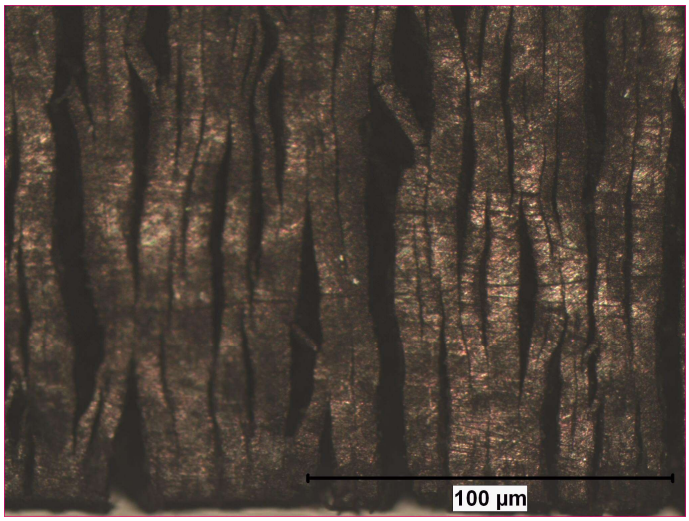

Figure 4.2-3. Optical Image of Homogenized (H) Sample obtained by Optical Microscope after 160th cycle (Last Cycle).

As the number of the cracks increased significantly at the 160th cycle and as the gage section of the sample decreased, the 15C/s heating and cooling rates were not maintained since the current, which passes through the sample cannot be controlled by the PI controller. Therefore, UCT and LCT values, which were set to PI controller, were not able to be kept at the set values. Overshooting and undercooling were observed. Therefore, the experiment was stopped at the end the 160th cycle without observing fracture. ε_{act} values were obtained from strain vs temperature curves and are illustrated in Figure 4.2-4. Generally speaking, ε_{act} values were determined to be lower than that of observed in other NiTiHf alloys which have less Hf content [8, 13]. ε_{act} values of H during cycles decreased sharply during the first couple of cycles started to increase till 45th cycle and stabilized at 0.8%. As the crack propagation and necking became very pronounced at around 150th cycle, a significant decrease was observed in the ε_{act}, as can be seen in Figure 4.2-4. ε_{mar} and ε_{aus} evolution of the H are given in Figure 4.2-5. Please note that, ε_{aus} is the accumulated ε_{irr} with the cycles of FFE and the ε_{act} is the difference between ε_{mar} and the ε_{aus}. As shown clearly in Figure 4.2-5, the ε_{aus} increased tremendously throughout FFE and reached to the level of 14% at the end of the 160th cycle.

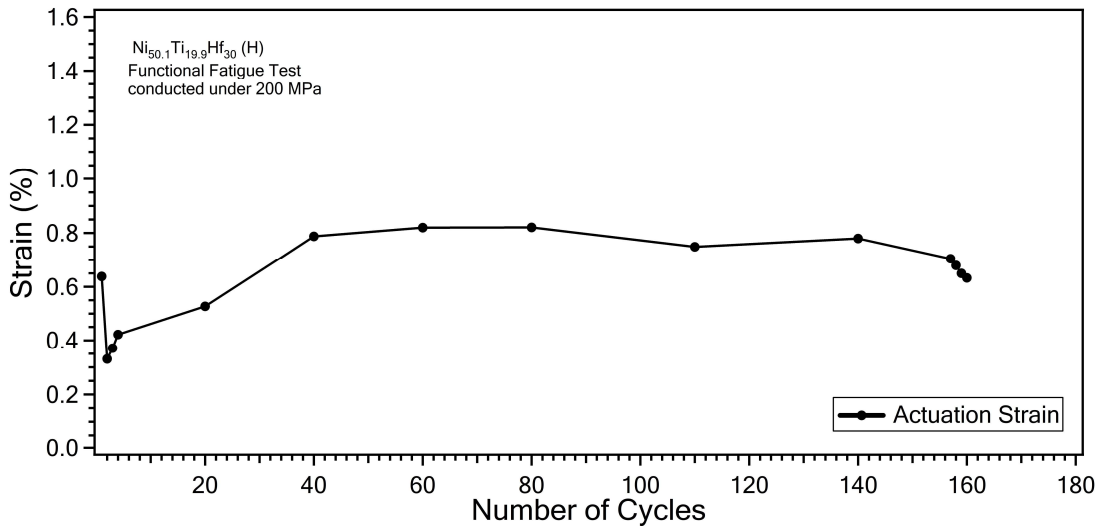

Figure 4.2-4. ε_{act} vs number of cycles for H, which were drawn using the data gathered during FFE.

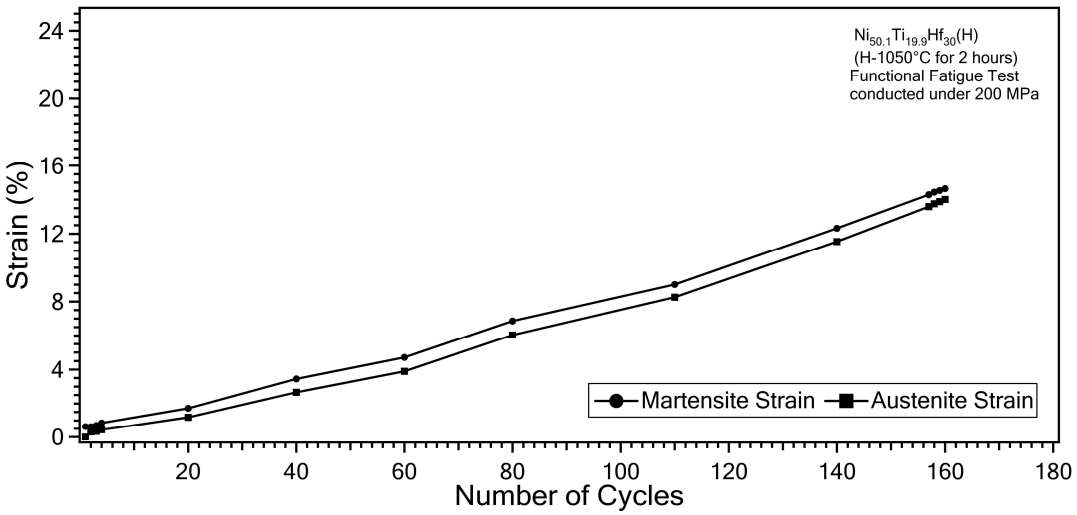

Figure 4.2-5. ε_{mar} and ε_{aus} (accumulated ε_{irr}) values as a function of cycles for homogenized (H) sample, which were determined from strain vs temperature curves of FFE.

Figure 4.2-6 and Table 4.2-1 demonstrate changes in TTs with the cycles for homogenized (H) sample. It was shown that TTs stayed stable up to 110^{th} cycle. However, after 110^{th} cycle, instabilities were observed in all TTs. This can be attributed to the very difficult control of heating the sample with many cracks and high oxidation residue on the surface, which were shown in Figure 4.2-2 and 4.2-3. Close control of heating rate

and maintaining the same UCT during heating were not able to be possible due to incorrect reading of temperature from the surface of the cracked sample.

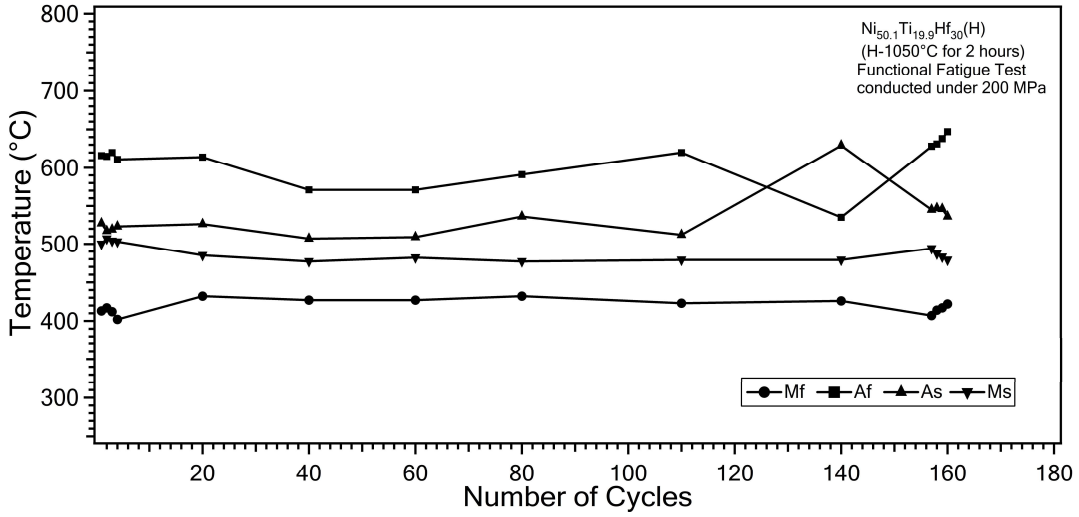

Figure 4.2-6. Evolution of TTs of Homogenized (H) sample with the number of cycles in FFE.

Table 4.2-1. TTs with the cycle numbers of homogenized (H) sample.

Number of Cycle	As (°C)	Af(°C)	Ms(°C)	Mf(°C)
1	527	616	500	413
2	517	615	507	417
3	519	620	504	412
4	523	611	503	402
20	526	614	485	432
40	507	571	477	427
60	509	571	482	427
80	536	591	477	432
110	512	620	479	423

Number of Cycle	As (°C)	Af(°C)	Ms(°C)	Mf(°C)
140	629	535	479	426
157	545	628	494	407
158	547	631	487	414
159	546	638	483	417
160	536	647	479	422

The strain-temperature behavior of H-WR2-500 sample is shown in Figure 4.2-5.

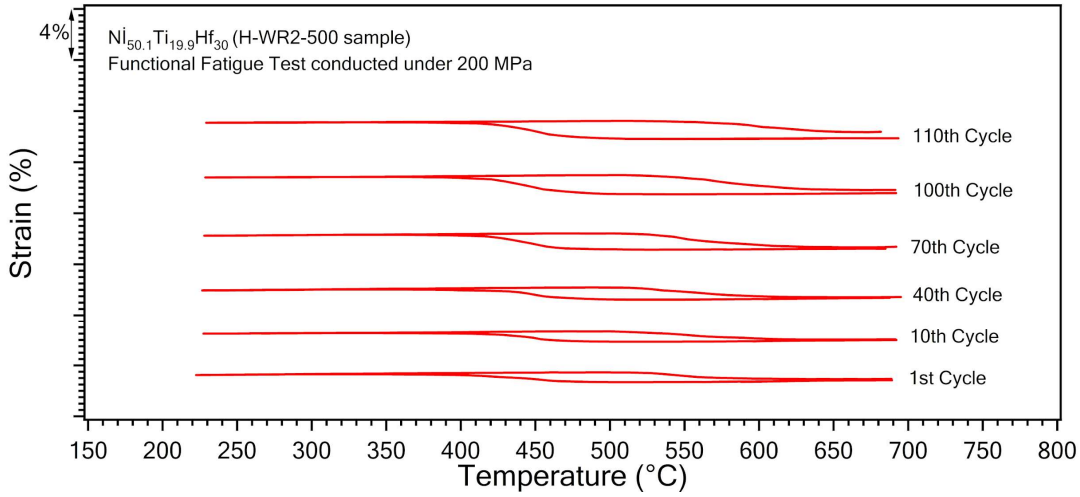

Figure 4.2-5. Strain - Temperature responses for (H-WR2-500) obtained from FFE.

When warm rolling was conducted on the sample, cracks were determined on the surface. The shallow cracks were smoothly grinded before running FFE. However, there could be inner cracks, which was able to be determined. These cracks were propagated during cycles. Figure 4.2-6 demonstrated the cracks which were propagated through the width of the FF samples. Additionally, it is clearly seen that the severe oxidation layer has formed in this sample as well. Other observations from these optical images were the crack formations on the oxide layers and their fiber separation kind of appearance.

Figure 4.2-6. Optical Images H-WR2-500 Sample, which were taken at the end of, (a) 50th Cycle (b) 110th Cycle (Last Cycle).

As illustrated in Figure 4.2-7, ε_{act} showed an increasing tendency, except at the beginning and the end of FFE. A decrease was observed during first 10 cycles and last 5 cycles. Actually, the decrease in the ε_{act} is the expected trend since the dislocations formed with the martensite-austenite transformation should lead to a decrease in the transforming volume. Besides, the increase in ε_{act} through most of the cycles can be attributed to very high UCT, which accelerated the crack formations and propagations, and the cyclic opening and closing of the cracks in this alloy, which occurred with phase transformations, one by one.

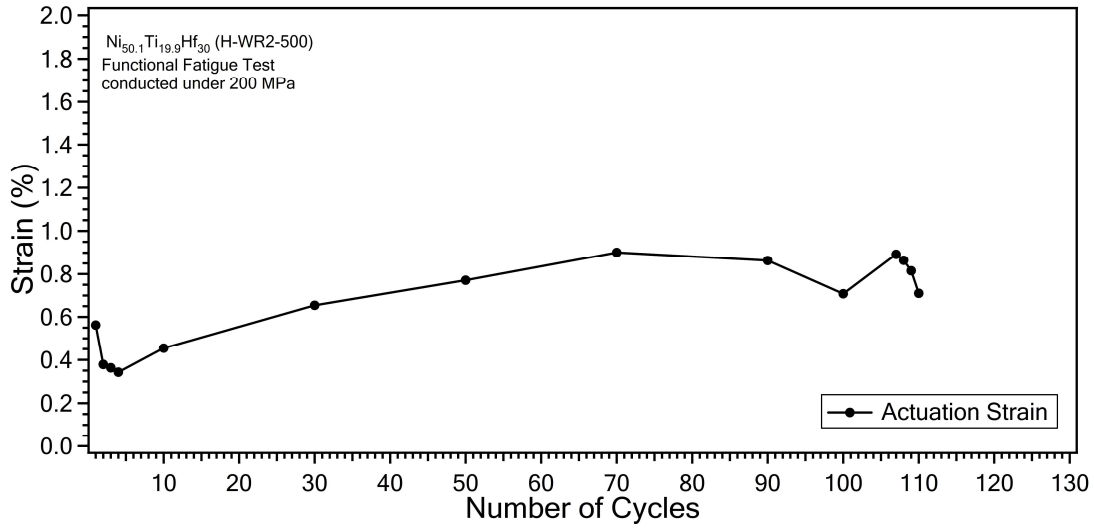

Figure 4.2-7. ε_{act} vs number of cycles for H-WR2-500 sample, which were drawn using the data gathered during FFE.

Changes in TTs of H-WR2-500 with respect to number of cycles were shown in Figure 4.2-8 and in Table 4.2-3. TTs were observed to be relatively stable with respect to the TTs evolution of H. Crack propagations and high operating temperature prevent TTs from changing significantly. M_f and A_f temperatures increased and M_s and A_s temperatures decreased during first 5 cycles and then all of them became stable. The instability of the TTs was also observed during the last 5 cycles due to again difficulty in measuring the sample temperature.

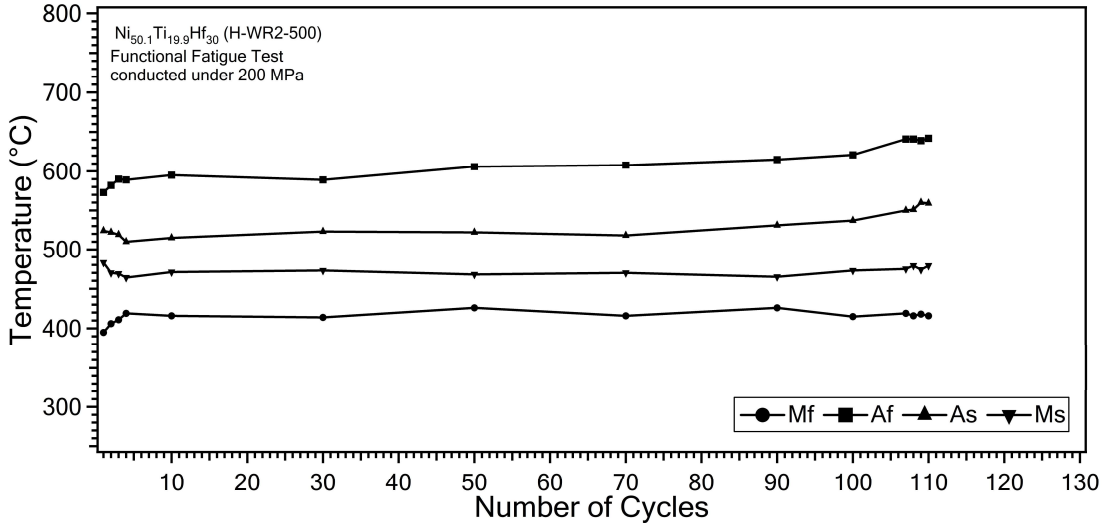

Figure 4.2-8. Evolution of TTs of H-WR2-500 sample with the number of cycles in FFE.

Table 4.2-2. TTs with the cycle numbers of H-WR2-500 sample.

Number of Cycle	As (°C)	Af(°C)	Ms(°C)	Mf(°C)
1	524	573	483	395
2	522	582	470	406
3	519	590	469	411
4	510	589	464	419
10	515	595	471	416
30	523	589	473	414

Number of Cycle	As (°C)	Af(°C)	Ms(°C)	Mf(°C)
50	522	606	468	426
70	518	608	470	416
90	531	615	465	426
100	537	621	473	415
107	550	641	475	419
108	551	641	479	416
109	560	639	474	418
110	559	642	479	416
Difference (°C) (110^{th} -1^{st})	35	69	-4	21

ε_{aus} (accumulated ε_{irr}) and ε_{mar} values, which were obtained from strain-temperature response of H-WR2-500 sample are shown in Figure 4.2-9. Total ε_{irr} value was determined as 14.71% at the last cycle for H-WR2-500 sample.

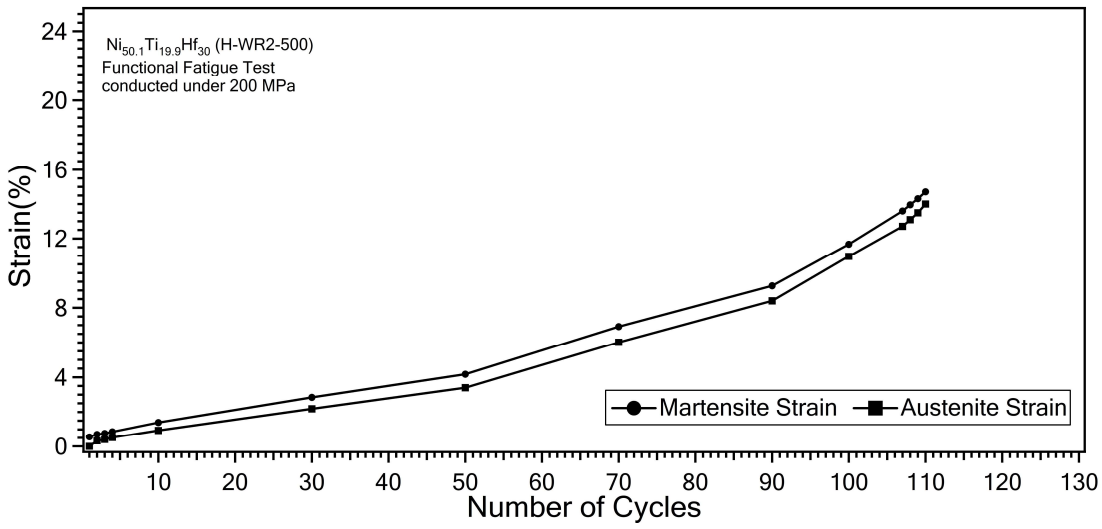

Figure 4.2-9. ε_{mar} and ε_{aus} (accumulated ε_{irr}) values as a function of cycles for H-WR2-500 sample, which were determined from strain -temperature curves of FFE.

Figure 4.2-10 demonstrates strain vs temperature curves, which were found from the FFE of H-WR10-800 sample. The sample was fractured after 150 cycles.

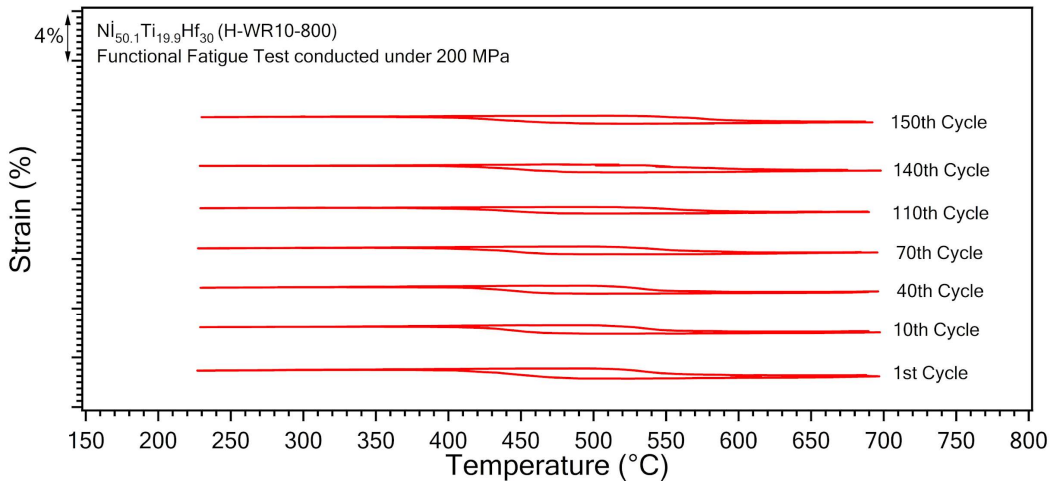

Figure 4.2-10. Strain -Temperature responses of H-WR10-800.

Figure 4.2-11 demonstrates change in ε_{act} during cycles. It was observed that the ε_{act} values of the H-WR10-800 sample were almost stayed constant with the possible higher dislocation density and the internal stress with warm rolling process with a higher thickness reduction. One another indication in the increase of dislocation density and the internal stress is the lower ε_{act} values as shown in Figure 4.12-13. Thickness reduction of this sample was more than that of the H-WR2-500 sample. Additionally, rolling process may induce texture and this texture may result to observe less ε_{act}. However, texture analysis with "X-Ray Diffraction" or "Electron Back Scattering Diffraction" methods should be done to prove the texture formation since the rolling temperature is relatively high to produce texture.

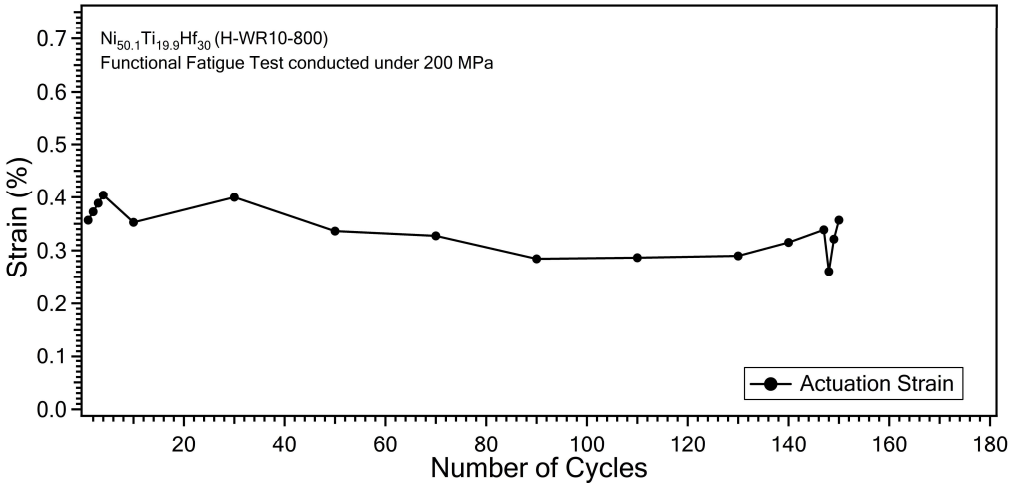

Figure 4.2-11. ε_{act} vs number of cycles for H-WR10-800 sample, which were drawn using the data gathered during FFE.

As shown in Figure 4.2-12 (a) there were cracks and oxidation layer on the surface of the sample after warm rolling. The surface cracks were removed via smooth grinding operation. Fiber separation kind of crack formations and oxidation of the surface throughout cycles were demonstrated in Figure 4.2-13 (a) and (b).

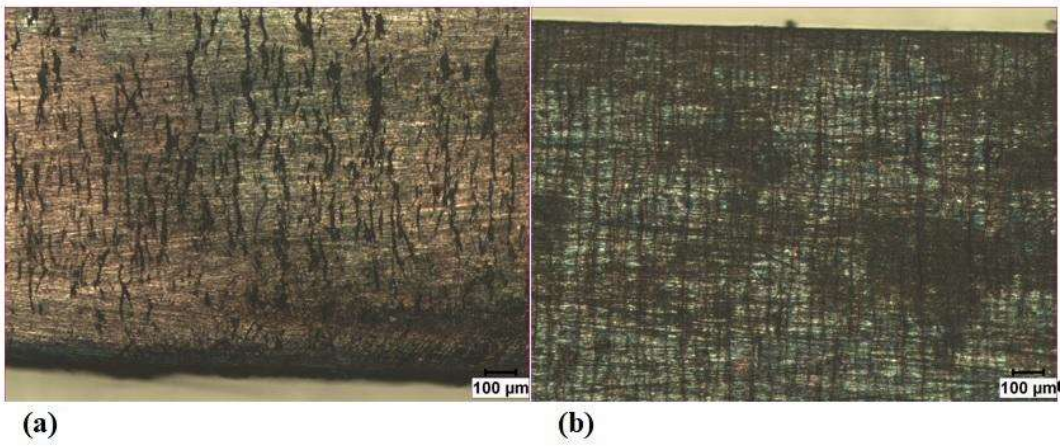

Figure 4.2-12. Optical Images H-WR10-800 Sample, which were taken, **(a)** after warm rolling process and **(b)at** the end of 40th Cycle.

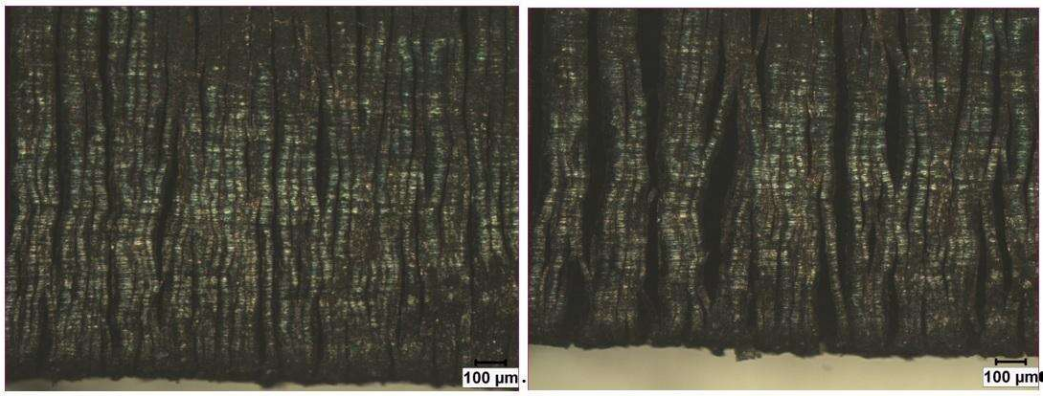

Figure 4.2-13. Optical Images H-WR10-800 Sample, which were taken at the end of, **(a)** 120th Cycle and **(b)** 150th Cycle (Last Cycle).

Changes in TTs during cycles for the H-WR10-800 sample were shown in Figure 4.2-14 and tabulated in Table 4.2-4. There was no significant change in M_s and M_f temperatures throughout cycles. The change in A_s and A_f temperatures were seen to be relatively higher than that of M_s and M_f temperatures and this might be attributed again the difficulty in measuring high temperatures from the surface of the cracked sample.

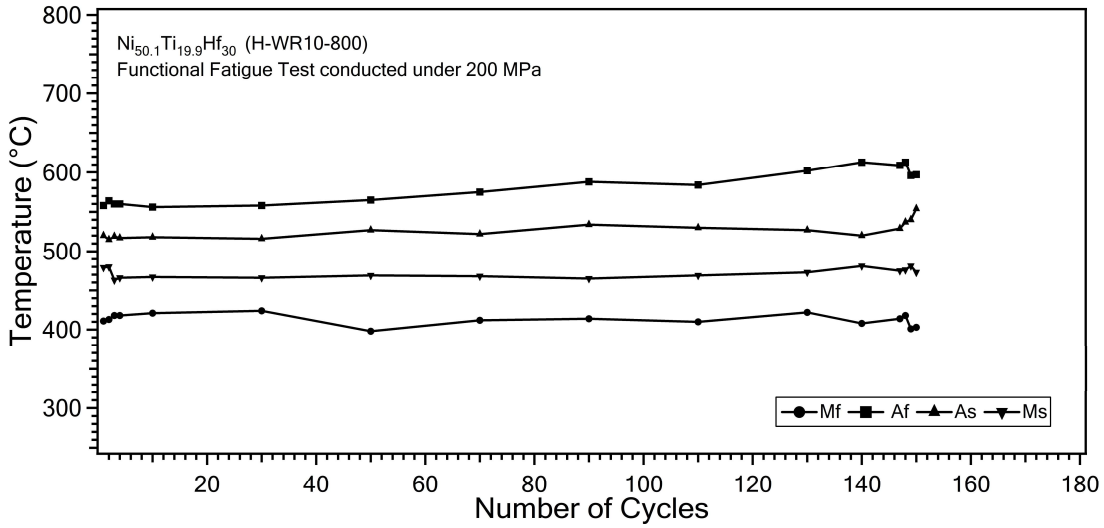

Figure 4.2-14. Evolution of TTs of H-WR10-800 sample with the number of cycles in FFE.

Table 4.2-3. TTs with the cycle numbers of H-WR10-800 sample.

Cycle	A_s(°C)	A_f(°C)	M_s(°C)	M_f(°C)
1	520	558	479	411
2	515	564	480	413
3	519	560	463	418
4	517	560	466	418
10	518	556	467	421
30	516	558	466	424
50	527	565	469	398
70	522	575	468	412
90	534	588	465	414
110	530	584	469	410
130	527	602	473	422
140	520	613	481	408
147	529	609	475	414
148	537	613	476	418
149	540	596	481	401
150	554	597	473	403
Difference (°C) (150^{th} -1^{st})	34	39	-6	-8

ε_{aus} (accumulated ε_{irr}) of H-WR10-800 sample and the total ε_{mar} with respect to cycles were shown in Figure 4.2-15. Total ε_{irr} was determined as 9.51% at the last cycle of FFE conducted on H-WR10-800 sample. As can be clearly seen, the accumulated ε_{irr} values were quite low, however, it should be noted that the ε_{act} values of this sample were also very low.

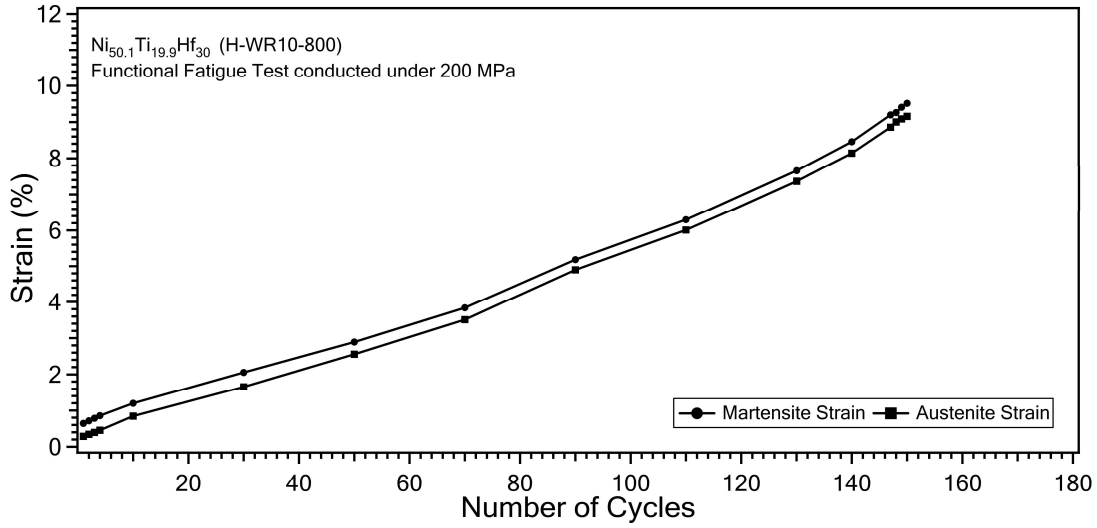

Figure 4.2-15. ε_{mar} and ε_{aus} (accumulated ε_{irr}) values as a function of cycles for H-WR10-800 sample, obtained from FFE.

Figure 4.2-16 shows strain vs temperature curves of H-WR10-900. It was fractured after 100 cycles.

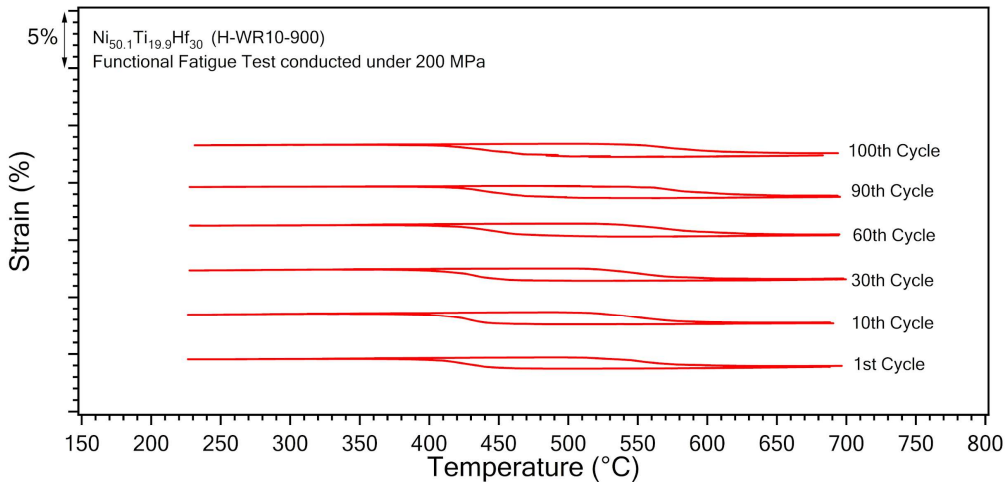

Figure 4.2-16. Strain -Temperature response of H-WR10-900.

Change in ε_{act} with the cycles, which were drawn from the FFE of H-WR10-900 is shown in Figure 4.2-17. First of all, it should be noted that the ε_{act} values were higher than that of the H-WR10-800 sample. Although the thickness reductions in both of the samples were the same, the warm rolling temperatures were different. 900°C warm rolling temperature may lead to a decrease in the induction of dislocation amount due to dynamic

recrystallization. However, the stability of the ε_{act} was maintained because of the induction of certain amount of dislocations.

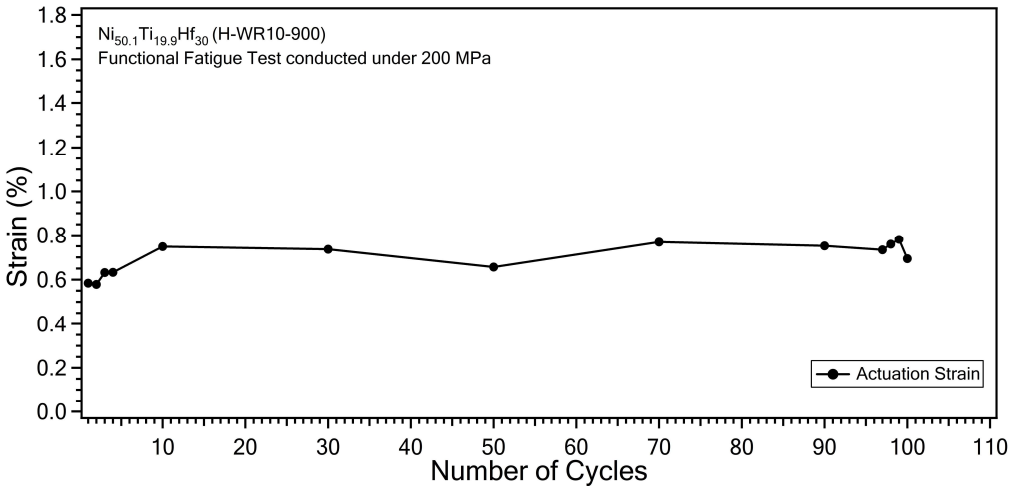

Figure 4.2-17. ε_{act} vs number of cycles for H-WR10-900 sample, which were drawn using the data gathered during FFE.

There were cracks and oxidations on the surface of the H-WR10-900 sample as well after WR. Although the sample was strengthened by dislocations ε_{act} was not reduced due to the fact that rolling temperature was enough for recrystallisation. Recrystallisation was reduced the amount of dislocations. Cracks and crack propagation images were shown in Figure 4.2-18 (a) and (b). Since H-WR10-900 sample was WR at 900°C the oxidation was relatively severe. Therefore, the sample became brittle after the warm rolling process, and it was fractured earlier than that of H-WR10-800.

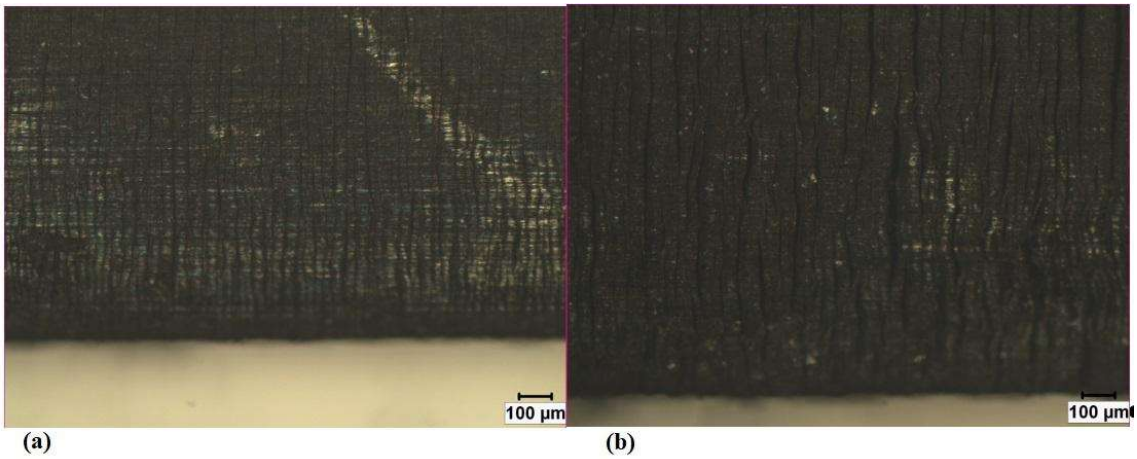

Figure 4.2-18. Optical Images H-WR10-900 Sample, which were taken **(a)** after 50th cycle and **(b)** after 100th cycle (Last Cycle).

Changes in TTs with the cycles, which were obtained strain vs temperature graphs for the H-WR10-900 sample are shown in Figure 4.2-19 and also tabulated in Table 4.2-5. TTs values and evolution were determined as similar to the values obtained from the FFE of H-WR10-800 sample.

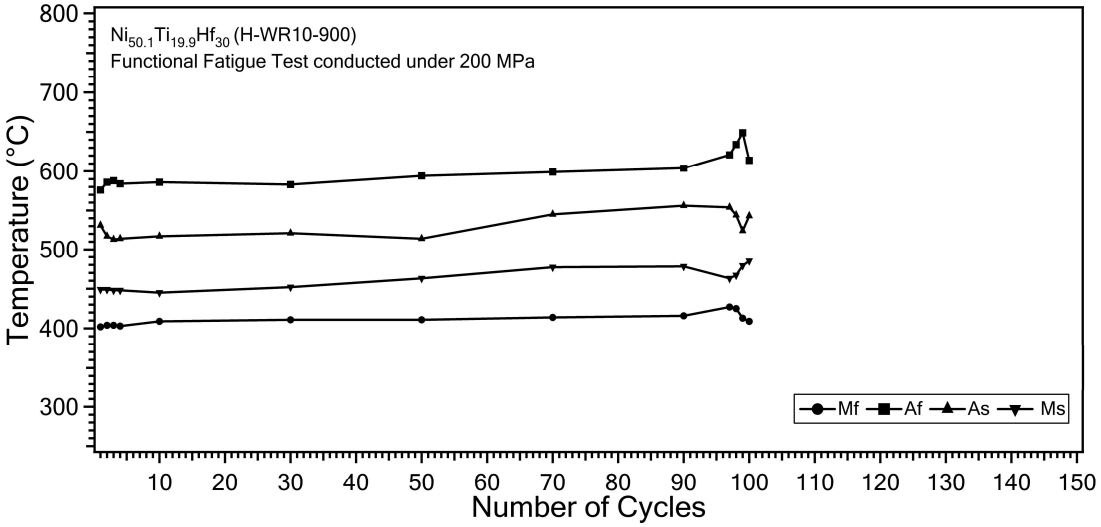

Figure 4.2-19. Evolution of TTs of H-WR10-900 sample with the number of cycles in FFE.

Table 4.2-4. TTs with the cycle numbers of H-WR10-900 sample.

Cycle	**A_s(°C)**	**A_f(°C)**	**M_s(°C)**	**M_f(°C)**
1	531	576	449	402
2	517	586	449	404
3	513	588	448	404
4	514	584	448	403
10	517	586	445	409
30	521	583	452	411
50	514	594	463	411
70	545	599	477	414
90	556	604	478	416
97	554	621	463	427
98	544	634	467	425
99	524	649	479	413
100	543	614	485	409
Difference(°C) (100^{th} -1^{st} Cycle)	12	38	36	7

ε_{aus} (accumulated ε_{irr}) and ε_{mar} values of H-WR10-900 sample during cycles are demonstrated in Figure 4.2-22. Total ε_{irr} was found as 9.48% after the last cycle for the H-WR10-900 sample.

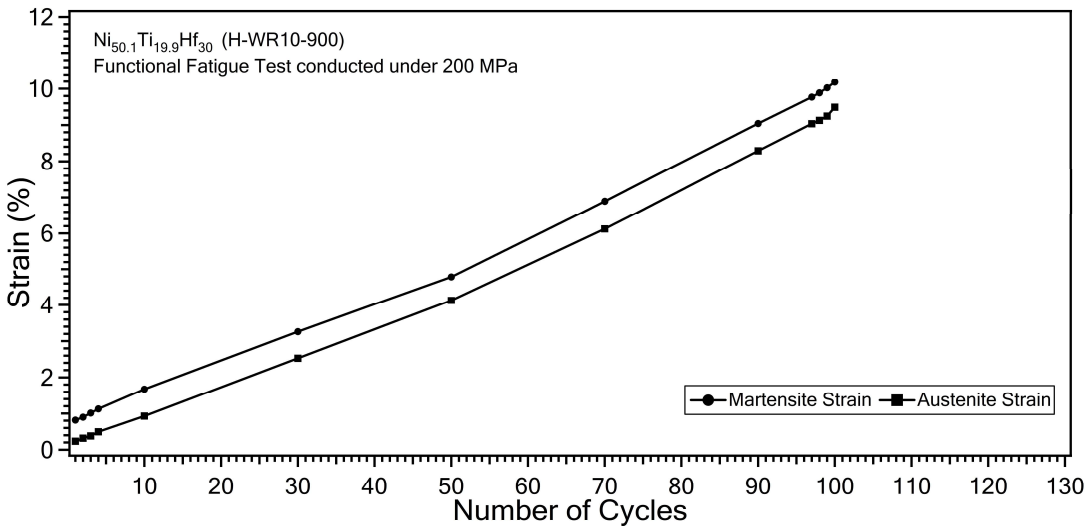

Figure 4.2-20. ε_{mar} and ε_{aus} (accumulated ε_{irr}) values as a function of cycles for H-WR10-900 sample, which were determined from strain vs temperature curves of FFE.

To better clarify the effect of warm rolling process, comparisons of FFE results of all samples are presented in this section. ε_{act} values of H, H-WR2-500, H-WR10-800, and H-WR10-900 samples were compared and are shown in Figure 4.2-21. H and H-WR2-500 samples had nearly the same ε_{act} values and the values increased with the number of cycles. 2% thickness reduction was not adequate to achieve stability in ε_{act}. ε_{act} values were reduced significantly by the application of warm rolling at 800°C with 10% thickness reduction. There might be two reasons for observing lower ε_{act} values. One is the increase in dislocation density with 10% thickness reduction and the other one is the texture formation with rolling. However, texture formation might not be possible via applying deformation at relatively higher temperatures as aforementioned. Further texture analysis should be done to affirm this reason. ε_{act} values of H-WR10-900 sample were found to be higher than that of H-WR10-800 in spite of having the same thickness reduction and this might be due to the dynamic recrystallization. Dynamic recrystallization may lead to attain less dislocation storage.

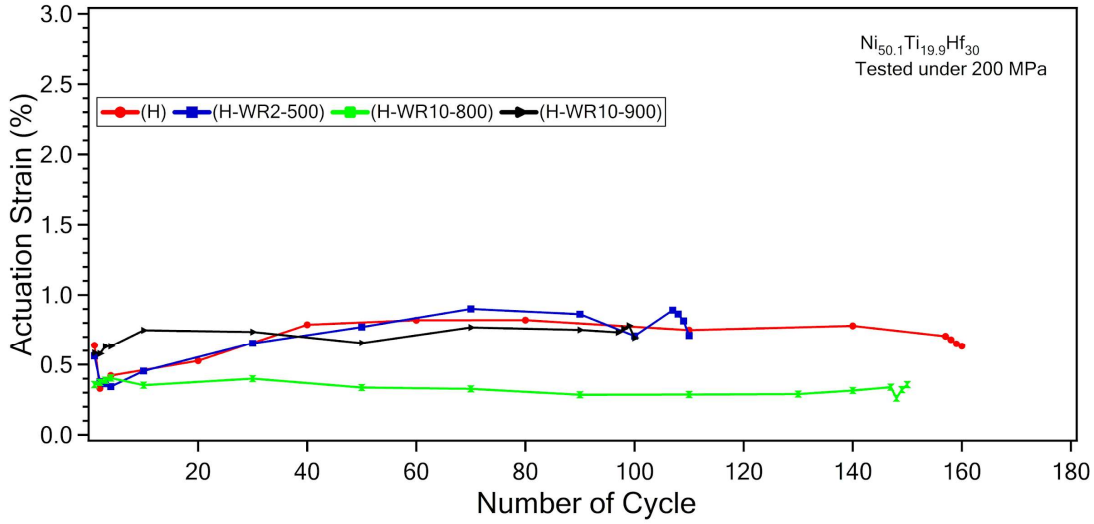

Figure 4.2-21. Comparison of ε_{act} values of H, H-WR2-500, H-WR10-800, and H-WR10-900 samples.

(b)

Figure 4.2-22 (a) and (b). The most important observation is the increased stability after rolling processes. Additionally, warm rolling led to a decrease in TTs of the alloy. This decrease can be seen by looking at the first cycles of the FFE. Since TTs of the H showed a decreasing tendency TTs of H and WRed samples reached to similar levels with the cycles.

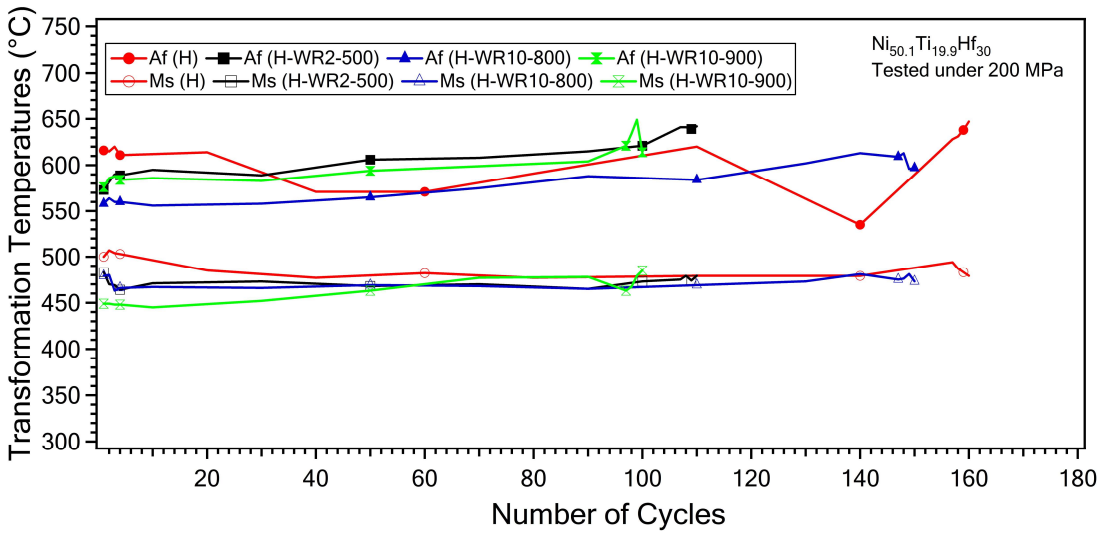

(a)

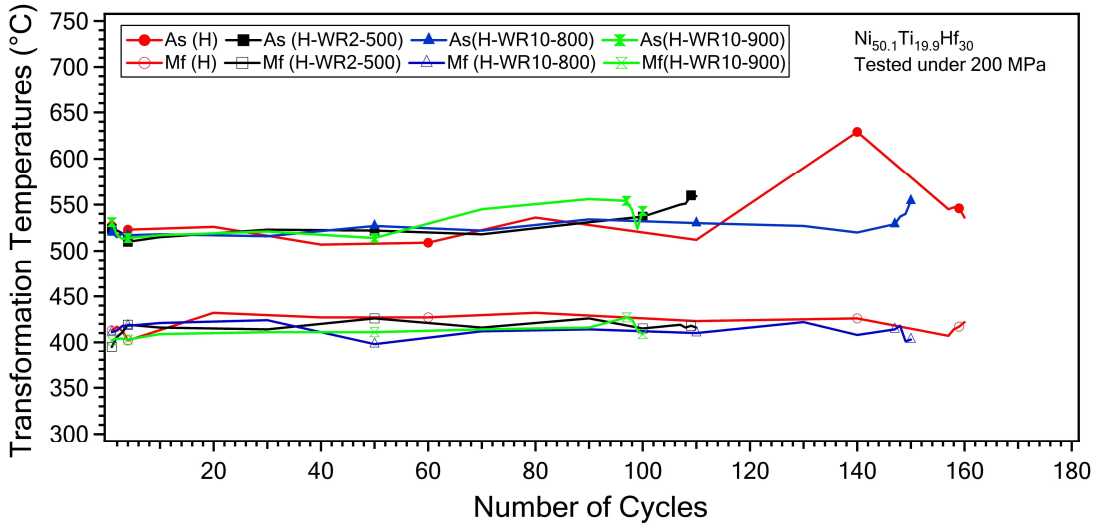

(b)

Figure 4.2-22. Comparison of TTs of all samples, which are H, H-WR2-500, H-WR10-800, and H-WR10-900 (a) A_f and M_s (b) A_s and M_f.

Addition to the comparisons of ε_{act} and TTs, T_{hyst} values were also compared for all samples and are shown in Figure 4.2-26. It was shown in the figure that hysteresis values of WRed samples fluctuated in a narrow range after warm rolling. However, the instability of the T_{hyst} of H sample was observed to be very significant due to the evolution of the microstructure of the H with the number of cycles. Firstly, T_{hyst} decreased during first 60 cycles and then started to increase.

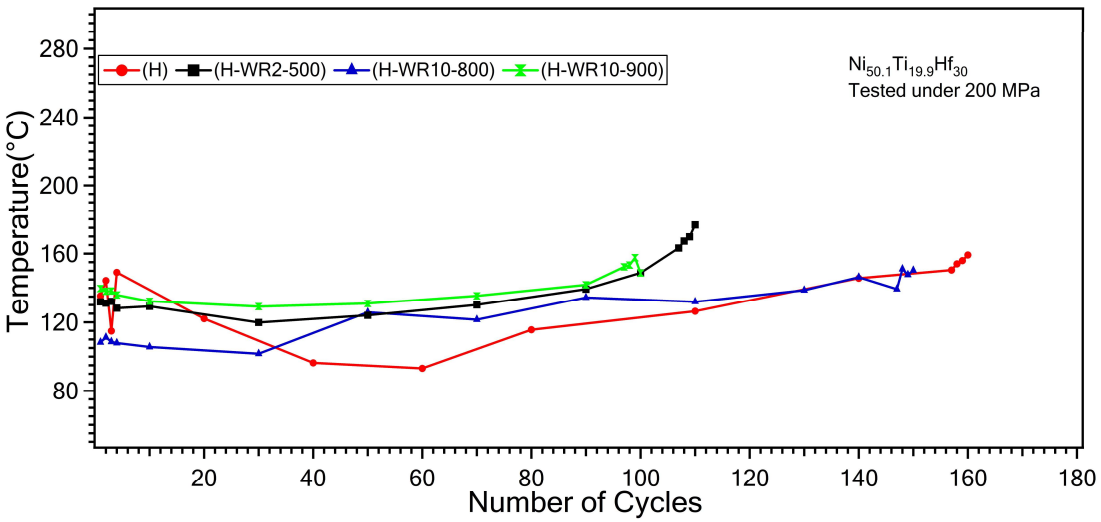

Figure 4.2-23. Comparison of T_{hyst} values of all samples during FFE.

Comparisons of ε_{mar} and ε_{aus} values of all samples were shown in Figure 4.2-24. The most intriguing finding is the observation of relatively lower accumulation ε_{irr} or in other terms ε_{aus} magnitudes in H-WR10-800. This is due to the fact that 10% thickness reduction at 800°C led to achieve higher dislocation density. Although the same observation was expected for the H-WR10-900 sample this sample showed higher accumulated ε_{irr} values with the number of cycles and this might be due to the dynamic recrystallization that led to less dislocation storage.

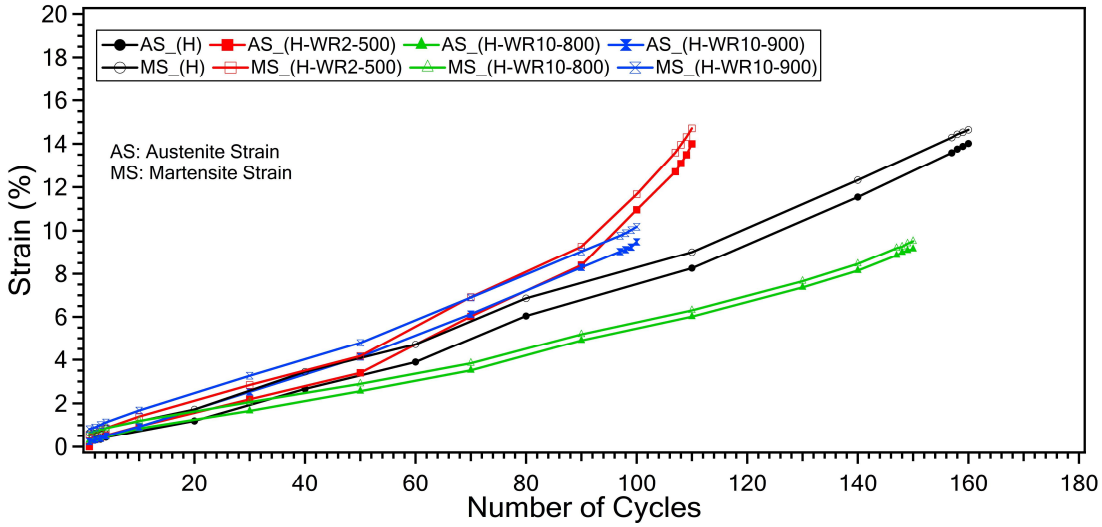

Figure 4.2-24. Comparison of ε_{mar} and ε_{aus} (Total ε_{irr}) for all samples during the cycles of H, H-WR2-500, H-WR10-800, and H-WR10-900.

5. CONCLUSION

Here are the conclusions which can be drawn from all the results, which were given in the previous section:

1) NiTiHf alloys with high Hf content are known as hard to deform materials. Although rolling processes were applied relatively at high temperatures in this study high percentages of thickness reduction were not achieved and crack formations were observed after warm rolling processes since Hf content of the alloy used in this study was quite high.
2) TTs of $Ni_{50.1}Ti_{19.9}Hf_{30}$ (at%) HTSMA were determined to be very high from DSC experiments. Therefore, FFEs were carried out at very high temperatures. UCTs in FFEs were set as 700°C and it was very difficult to measure these high temperatures during FFEs from the surface of the samples. Severe oxidation due to heating the samples to 700°C made the control of the heating rate very difficult. Thus, heating the samples to exactly 700°C, which was chosen as UCT for all samples, was not possible. Overshooting was generally comprised. Additionally, the crack formations and the propagations on the oxidized layers of the surface contributed to the difficulty of measuring sample temperature from the surface.
3) Despite all the difficulties in running FFEs, the thermal cycles under 200MPa stress magnitude were conducted on H, H-WR2-500, H-WR10-800, and H-WR10-900 samples and here are the most important findings from these FFEs.
    a) ε_{act} values $Ni_{50.1}Ti_{19.9}Hf_{30}$ (at%) alloy were determined to be quite low compared with the other NiTiHf alloys having less Hf content [8, 13].
    b) ε_{act} values were decreased down to 0.4% levels by the warm rolling process at 800°C with 10% thickness reduction due to the increased dislocation density which led to a decrease in transforming volume via pinning the martensite-austenite boundary. By increasing the warm rolling temperature, ε_{act} values increased again due to the dynamic recrystallization which led to less dislocation storage.
    c) The stability of ε_{act} values and TTs was increased with warm rolling process due to the increase in resistance to plasticity during phase transformation via the increase in dislocation density.

d) FLs after warm rolling process decreased although the stabilities of the functional properties of $Ni_{50.1}Ti_{19.9}Hf_{30}$ (at%) HTSMA were increased. This can be attributed to the crack formations with the rolling process and the ease of crack propagation with the further decrease in the ductility of $Ni_{50.1}Ti_{19.9}Hf_{30}$ (at%) HTSMA.

REFERENCES

[1] J. Ma, I. Karaman, and R. D. Noebe, "High temperature shape memory alloys," *International Materials Reviews*, vol. 55, no. 5, pp. 257–315, Sep. 2010.

[2] D. J. Hartl and D. C. Lagoudas, "Aerospace applications of shape memory alloys," *Proceedings of the Institution of Mechanical Engineers, Part G: Journal of Aerospace Engineering*, vol. 221, no. 4, pp. 535–552, Apr. 2007.

[3] J. M. Jani, M. Leary, and A. Subic, "Shape Memory Alloys in Automotive Applications," *Applied Mechanics and Materials*, vol. 663, pp. 248–253, Oct. 2014.

[4] F. el Feninat, G. Laroche, M. Fiset, and D. Mantovani, "Shape Memory Materials for Biomedical Applications," *Advanced Engineering Materials*, vol. 4, no. 3, pp. 91–104, Mar. 2002.

[5] K. Otsuka and X. Ren, "Physical metallurgy of Ti–Ni-based shape memory alloys," *Progress in Materials Science*, vol. 50, no. 5, pp. 511–678, Jul. 2005.

[6] B. Kockar, I. Karaman, J. I. Kim, Y. I. Chumlyakov, J. Sharp, and C.-J. (Mike) Yu, "Thermomechanical cyclic response of an ultrafine-grained NiTi shape memory alloy," *Acta Materialia*, vol. 56, no. 14, pp. 3630–3646, Aug. 2008.

[7] J. Mohd Jani, M. Leary, A. Subic, and M. A. Gibson, "A review of shape memory alloy research, applications and opportunities," *Materials & Design (1980-2015)*, vol. 56, pp. 1078–1113, Apr. 2014.

[8] H. O. Tugrul, H. H. Saygili, M. S. Velipasaoglu, and B. Kockar, "Comparison of the transformation behavior of cold rolling with aging and hot extrusion with aging processed $Ni_{50.3}$ $Ti_{29.7}$ Hf_{20} high temperature shape memory alloy," *Smart Materials and Structures*, vol. 28, no. 10, p. 105029, Oct. 2019.

[9] G. S. Firstov, J. van Humbeeck, and Yu. N. Koval, "High Temperature Shape Memory Alloys Problems and Prospects," *Journal of Intelligent Material Systems and Structures*, vol. 17, no. 12, pp. 1041–1047, Dec. 2006.

[10] M. Ataei, A. Zarei-Hanzaki, and A. Shamsolhodaei, "Shape memory response and mechanical properties of warm deformed NiTi intermetallic alloy," *Materials Science and Engineering: A*, vol. 680, pp. 291–296, Jan. 2017.

[11] N. Babacan, M. Bilal, C. Hayrettin, J. Liu, O. Benafan, and I. Karaman, “Effects of cold and warm rolling on the shape memory response of Ni50Ti30Hf20 high-temperature shape memory alloy,” *Acta Materialia*, vol. 157, pp. 228–244, Sep. 2018.

[12] M. Prasher, D. Sen, R. Tewari, P. S. R. Krishna, P. D. Babu, and M. Krishnan, “Effect of Hf solute addition on the phase transformation behavior and hardness of a Ni-rich NiTi alloy,” *Materials Chemistry and Physics*, vol. 247, p. 122890, Jun. 2020.

[13] H. H. Saygili, H. O. Tugrul, and B. Kockar, “Effect of Aging Heat Treatment on the High Cycle Fatigue Life of Ni50.3Ti29.7Hf20 High-Temperature Shape Memory Alloy,” *Shape Memory and Superelasticity*, vol. 5, no. 1, pp. 32–41, Mar. 2019.

[14] Velipasaoglu Mustafa Sefa, “The Determination of The Functional Fatigue Life of High Temperature Shape Memory Alloys After Cold Rolling Process,” Graduate School of Science and Engineering of Hacettepe University, Ankara, 2020.

[15] K. Otsuka and X. Ren, “Recent developments in the research of shape memory alloys,” *Intermetallics (Barking)*, vol. 7, no. 5, pp. 511–528, May 1999.

[16] W. Abuzaid and H. Sehitoglu, “Functional fatigue of Ni50.3Ti25Hf24.7 – Heterogeneities and evolution of local transformation strains,” *Materials Science and Engineering: A*, vol. 696, pp. 482–492, Jun. 2017.

[17] D. C. Lagoudas, *Shape Memory Alloys*, vol. 1. Boston, MA: Springer US, 2008.

[18] D. J. Hartl and D. C. Lagoudas, “Aerospace applications of shape memory alloys,” *Proceedings of the Institution of Mechanical Engineers, Part G: Journal of Aerospace Engineering*, vol. 221, no. 4, pp. 535–552, Apr. 2007.

[19] W. Abuzaid and H. Sehitoglu, “Functional fatigue of Ni50.3Ti25Hf24.7 – Heterogeneities and evolution of local transformation strains,” *Materials Science and Engineering: A*, vol. 696, pp. 482–492, Jun. 2017.

[20] T. B. Massalski, “Solid-state transformations in copper-based alloys,” *Metals Technology*, vol. 7, no. 1, pp. 300–304, Jan. 1980.

[21] R. Dasgupta, “A look into Cu-based shape memory alloys: Present scenario and future prospects,” *Journal of Materials Research*, vol. 29, no. 16, pp. 1681–1698, Aug. 2014.

[22] Saygili Hasan Huseyin, “The Development of a fatigue test machine to investigate the functional fatigue life of high temperature shape memory alloys and the

determination of the functional fatigue life of these alloys," Graduate School of Science and Engineering of Hacettepe University, Ankara, 2018.

[23] T. Maruyama and H. Kubo, "Ferrous (Fe-based) shape memory alloys (SMAs): properties, processing, and applications," in *Shape Memory and Superelastic Alloys*, Elsevier, 2011, pp. 141–159.

[24] H. E. Karaca *et al.*, "Shape memory behavior of high strength NiTiHfPd polycrystalline alloys," *Acta Materialia*, vol. 61, no. 13, pp. 5036–5049, Aug. 2013.

[25] H. Y. Kim, T. Jinguu, T. Nam, and S. Miyazaki, "Cold workability and shape memory properties of novel Ti–Ni–Hf–Nb high-temperature shape memory alloys," *Scripta Materialia*, vol. 65, no. 9, pp. 846–849, Nov. 2011.

[26] X. L. Meng, W. Cai, Y. D. Fu, J. X. Zhang, and L. C. Zhao, "Martensite structure in Ti–Ni–Hf–Cu quaternary alloy ribbons containing (Ti,Hf)2Ni precipitates," *Acta Materialia*, vol. 58, no. 10, pp. 3751–3763, Jun. 2010.

[27] X. L. Meng, W. Cai, K. T. Lau, L. C. Zhao, and L. M. Zhou, "Phase transformation and microstructure of quaternary TiNiHfCu high temperature shape memory alloys," *Intermetallics (Barking)*, vol. 13, no. 2, pp. 197–201, Feb. 2005.

[28] H. E. Karaca *et al.*, "Effects of nanoprecipitation on the shape memory and material properties of an Ni-rich NiTiHf high temperature shape memory alloy," *Acta Materialia*, vol. 61, no. 19, pp. 7422–7431, Nov. 2013.

[29] D. Golberg *et al.*, "Characteristics of Ti50Pd30Ni20 high-temperature shape memory alloy," *Intermetallics (Barking)*, vol. 3, no. 1, pp. 35–46, Jan. 1995,

[30] O. Benafan *et al.*, "Shape memory alloy actuator design: CASMART collaborative best practices and case studies," *International Journal of Mechanics and Materials in Design*, vol. 10, no. 1, pp. 1–42, Mar. 2014.

[31] E. T. F. Chau, C. M. Friend, D. M. Allen, J. Hora, and J. R. Webster, "A technical and economic appraisal of shape memory alloys for aerospace applications," *Materials Science and Engineering: A*, vol. 438–440, pp. 589–592, Nov. 2006,

[32] L. McDonald Schetky, "Shape memory alloy applications in space systems," *Materials & Design*, vol. 12, no. 1, pp. 29–32, Feb. 1991.

[33] J. van Humbeeck, "Non-medical applications of shape memory alloys," *Materials Science and Engineering: A*, vol. 273–275, pp. 134–148, Dec. 1999.

[34] A. W. Young, R. W. Wheeler, N. A. Ley, O. Benafan, and M. L. Young, "Microstructural and Thermomechanical Comparison of Ni-Rich and Ni-Lean

NiTi-20 at. % Hf High Temperature Shape Memory Alloy Wires," *Shape Memory and Superelasticity*, vol. 5, no. 4, pp. 397–406, Dec. 2019.

[35] S. Barbarino, E. I. Saavedra Flores, R. M. Ajaj, I. Dayyani, and M. I. Friswell, "A review on shape memory alloys with applications to morphing aircraft," *Smart Materials and Structures*, vol. 23, no. 6, p. 063001, Jun. 2014.

[36] R. HOLTZ, "Fatigue thresholds of Ni-Ti alloy near the shape memory transition temperature," *International Journal of Fatigue*, vol. 21, pp. 137–145, Sep. 1999,

[37] N. Simiriotis, M. Fragiadakis, J. F. Rouchon, and M. Braza, "Shape control and design of aeronautical configurations using shape memory alloy actuators," *Computers & Structures*, vol. 244, p. 106434, Feb. 2021.

[38] C. M. Denowh and D. A. Miller, "Thermomechanical training and characterization of Ni–Ti–Hf and Ni–Ti–Hf–Cu high temperature shape memory alloys," *Smart Materials and Structures*, vol. 21, no. 6, p. 065020, Jun. 2012.

[39] K. C. Atli, I. Karaman, R. D. Noebe, G. Bigelow, and D. Gaydosh, "Work production using the two-way shape memory effect in NiTi and a Ni-rich NiTiHf high-temperature shape memory alloy," *Smart Materials and Structures*, vol. 24, no. 12, p. 125023, Dec. 2015.

[40] B. Amin-Ahmadi, T. Gallmeyer, J. G. Pauza, T. W. Duerig, R. D. Noebe, and A. P. Stebner, "Effect of a pre-aging treatment on the mechanical behaviors of Ni50.3Ti49.7−xHfx (x ≤ 9 at. %) Shape memory alloys," *Scripta Materialia*, vol. 147, pp. 11–15, Apr. 2018.

[41] M. I. Khan, H. Y. Kim, Y. Namigata, T. Nam, and S. Miyazaki, "Combined effects of work hardening and precipitation strengthening on the cyclic stability of TiNiPdCu-based high-temperature shape memory alloys," *Acta Materialia*, vol. 61, no. 13, pp. 4797–4810, Aug. 2013.

[42] H. E. Karaca, E. Acar, H. Tobe, and S. M. Saghaian, "NiTiHf-based shape memory alloys," *Materials Science and Technology*, vol. 30, no. 13, pp. 1530–1544, Nov. 2014.

[43] Y. Wang, "The tensile behavior of Ti36Ni49Hf15 high temperature shape memory alloy," *Scripta Materialia*, vol. 40, no. 12, pp. 1327–1331, May 1999.

[44] S. Besseghini, E. Villa, and A. Tuissi, "Ni□Ti□Hf shape memory alloy: effect of aging and thermal cycling," *Materials Science and Engineering: A*, vol. 273–275, pp. 390–394, Dec. 1999.

[45] D. R. Angst, P. E. Thoma, and M. Y. Kao, “The Effect of Hafnium Content on the Transformation Temperatures of Ni $_{49}$ Ti $_{51-x}$ Hf $_{x}$. Shape Memory Alloys,” *Journal de Physique IV*, vol. 05, no. C8, pp. C8-747-C8-752, Dec. 1995.

[46] P. E. T. M. Y. K. and D. R. A. D. Abu Judom, “High transformation temperature shape memory alloy,” 1992.

[47] M. Frost, B. Benešová, H. Seiner, M. Kružík, P. Šittner, and P. Sedlák, “Thermomechanical model for NiTi-based shape memory alloys covering macroscopic localization of martensitic transformation,” *International Journal of Solids and Structures*, vol. 221, pp. 117–129, Jun. 2021.

[48] D. C. Lagoudas, D. A. Miller, L. Rong, and P. K. Kumar, “Thermomechanical fatigue of shape memory alloys,” *Smart Materials and Structures*, vol. 18, no. 8, p. 085021, Aug. 2009.

[49] O. W. Bertacchini, D. C. Lagoudas, F. T. Calkins, and J. H. Mabe, “Thermomechanical cyclic loading and fatigue life characterization of nickel rich NiTi shape-memory alloy actuators,” Mar. 2008, p. 692916.

[50] H. Hosoda *et al.*, “Cold rolling of B2 intermetallics,” *Journal of Alloys and Compounds*, vol. 302, no. 1–2, pp. 266–273, Apr. 2000.

[51] M. E. Mitwally and M. Farag, “Effect of cold work and annealing on the structure and characteristics of NiTi alloy,” *Materials Science and Engineering: A*, vol. 519, no. 1–2, pp. 155–166, Aug. 2009.

[52] N. A. Ley, R. W. Wheeler, O. Benafan, and M. L. Young, “Characterization of Thermomechanically Processed High-Temperature Ni-Lean NiTi–20 at. % Hf Shape Memory Wires,” *Shape Memory and Superelasticity*, vol. 5, no. 4, pp. 476–485, Dec. 2019.

[53] O. Karakoc, C. Hayrettin, D. Canadinc, and I. Karaman, “Role of applied stress level on the actuation fatigue behavior of NiTiHf high temperature shape memory alloys,” *Acta Materialia*, vol. 153, pp. 156–168, Jul. 2018.

[54] A. Ahadi, E. Rezaei, and A. Karimi Taheri, “Effect of hot rolling on microstructure and transformation cycling behaviour of equiatomic NiTi shape memory alloy,” *Materials Science and Technology*, vol. 28, no. 6, pp. 727–732, Jun. 2012.

[55] O. Akgul, H. O. Tugrul, and B. Kockar, “Effect of the cooling rate on the thermal and thermomechanical behavior of NiTiHf high-temperature shape memory alloy,” *Journal of Materials Research*, vol. 35, no. 12, pp. 1572–1581, Jun. 2020.